HAL
open science

The role of H2O on metamorphism and deformation at high pressure: A combined petrological and thermo-mechanical study based on the Gran Paradiso Unit, Western Alps

Cindy Luisier, Michel Ballèvre, Thibault Duretz

To cite this version:

Cindy Luisier, Michel Ballèvre, Thibault Duretz. The role of H2O on metamorphism and deformation at high pressure: A combined petrological and thermo-mechanical study based on the Gran Paradiso Unit, Western Alps. Lithos, 2023, 446, pp.107123. 10.1016/j.lithos.2023.107123 . insu-04038873

HAL Id: insu-04038873

https://insu.hal.science/insu-04038873v1

Submitted on 21 Mar 2023

HAL is a multi-disciplinary open access archive for the deposit and dissemination of scientific research documents, whether they are published or not. The documents may come from teaching and research institutions in France or abroad, or from public or private research centers.

L'archive ouverte pluridisciplinaire **HAL**, est destinée au dépôt et à la diffusion de documents scientifiques de niveau recherche, publiés ou non, émanant des établissements d'enseignement et de recherche français ou étrangers, des laboratoires publics ou privés.

Journal Pre-proof

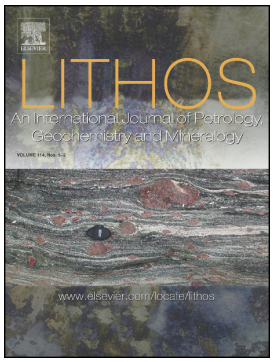

The role of H2O on metamorphism and deformation at high pressure: A combined petrological and thermo-mechanical study based on the Gran Paradiso Unit, Western Alps

Cindy Luisier, Michel Ballèvre, Thibault Duretz

PII: S0024-4937(23)00107-X

DOI: https://doi.org/10.1016/j.lithos.2023.107123

Reference: LITHOS 107123

To appear in: *LITHOS*

Received date: 30 March 2022

Revised date: 6 March 2023

Accepted date: 9 March 2023

Please cite this article as: C. Luisier, M. Ballèvre and T. Duretz, The role of H2O on metamorphism and deformation at high pressure: A combined petrological and thermo-mechanical study based on the Gran Paradiso Unit, Western Alps, *LITHOS* (2023), https://doi.org/10.1016/j.lithos.2023.107123

This is a PDF file of an article that has undergone enhancements after acceptance, such as the addition of a cover page and metadata, and formatting for readability, but it is not yet the definitive version of record. This version will undergo additional copyediting, typesetting and review before it is published in its final form, but we are providing this version to give early visibility of the article. Please note that, during the production process, errors may be discovered which could affect the content, and all legal disclaimers that apply to the journal pertain.

© 2023 Published by Elsevier B.V.

Journal Pre-proof

The role of H_2O on metamorphism and deformation at high pressure: a combined petrological and thermo-mechanical study based on the Gran Paradiso Unit, Western Alps

Cindy Luisier[1,2], Michel Ballèvre[1], Thibault Duretz[1,2]

[1]Université de Rennes, CNRS, Géosciences Rennes UMR 6118, Rennes, France

[2]Institut für Geowissenschaften, Goethe-Universität Frankfurt, Frankfurt am Main, Germany

Corresponding author:

Cindy Luisier

Goethe-Universität Frankfurt

Institut für Geowissenschaften

Altenhöferallee 1

60438 Frankfurt am Main

cindy.luisier@gmail.com

Journal Pre-proof

Abstract

Quantitative phase petrology analysis of two samples showing variable strain record and different peak pressure (*P*) conditions show that H_2O is a key parameter in the development of contrasting high-pressure (H*P*) peak conditions in adjacent polymetamorphic rocks. A shear zone in a paragneiss from the Gran Paradiso nappe, Western Alps, shows an Alpine foliation and records a peak *P* of 1.9 GPa, for a temperature of 500 to 520 °C. A few tens of meters away from the shear zone, a paragneiss showing no apparent Alpine age deformation records a peak *P* of maximum 1.4 GPa for the temperature range of 500 to 520 °C. The H_2O content of the latter has potentially been reduced to low contents following the pre-Alpine, Variscan amphibolite facies, and the absence of re-hydration prior to Alpine orogeny could have inhibited the formation of H*P* mineral assemblages. The validity of this interpretation is questioned here by considering the mechanical effect of H_2O undersaturated rocks on deformation and *P* during deformation. Based on a thermo-mechanical numerical modelling study, we show that heterogeneities in fluid saturation conditions between rocks lead to strength contrasts that are sufficient to trigger a dynamic *P* in the range of several hundreds of MPa. In particular, the models successfully reproduce the measured peak *P* between the two paragneiss studied. This model could be applied to other H_2O deficient rocks from H*P* tectonic units to further explore the role of H_2O on the rheology and hence assess its potential impact in the preservation of low *P* bodies in otherwise H*P* units from continental collision settings.

keywords:

high-pressure metamorphism, Gran Paradiso Unit, fluids, kinetics, rheology, thermo-mechanical modelling, thermodynamic modelling

Journal Pre-proof

Introduction

Metamorphic transformations in rocks occur due to spatial-temporal variations in environmental factors such as pressure (*P*), temperature (*T*), fluid availability and composition (Fyfe et al., 1978). In regional metamorphic environments, a change of these intensive (*P*, *T*) and extensive (fluid availability and rock composition) variables takes place due to the burial of the subducting lithosphere during ongoing convergence and triggers changes in metamorphic mineral parageneses. Along with mineral transformations, fluids may be released, through destabilization of hydrous minerals (Schmidt and Poli, 1998) and percolate along lithological interfaces and areas of enhanced permeability (e.g., Connolly and Podladchikov, 2013). Fluid-rock interactions may in turn lead to further modifications of the original rock composition through metasomatism. The mechanical behavior of rocks under stress depends on their rheology, mainly because minerals have different responses to deviatoric stress. Witnesses of the effect on deviatoric stress is recorded in rocks by deformation patterns, such as foliation, lineation, strain shadows around minerals, etc., as well as deformation mechanisms in minerals (fracturing, twinning, diverse types of recrystallisation; e.g., Passchier and Trouw, 2005). Although it is commonly accepted that the presence of a deviatoric component of stress implies that the stress state is not hydrostatic, the magnitude of the deviation from the hydrostatic stress and hence from the lithostatic *P* (i.e., the vertical stress component) is difficult to quantify.

Although the large-scale burial of rock units in convergent systems can be seen as a continuous process in time and space, *P* and *T* can be locally heterogeneous (Schenker et al., 2015). Disturbances of the *P* and *T* values are mainly controlled by the ability of rocks to deform under tectonic stress (Mancktelow, 2008; Schmalholz and Podladchikov, 2014). For example, shear deformation induces shear heating, which can locally increase the temperature

by up 50 to 150 °C (Kiss et al., 2019). As rocks are heterogeneous from the sample scale to the nappe scale, deformation induces stress perturbations, which, in turn, can result in local *P* deviations from the lithostatic value (e. g., Jamtveit et al., 2018; Luisier, 2018; Mancktelow, 1995; Moulas et al., 2013). Evidences are based on field observations, structural reconstructions and petrological studies in orogenic systems worldwide (e. g., Chu et al., 2017; Vaughan-Hammon et al., 2021; Vrijmoed et al., 2009). However, on the other hand, it has been suggested that metamorphic transformations do not occur in H_2O deficient rocks because of the slow reaction kinetics under H_2O deficient conditions (i.e., metastability with respect to the new *P-T* conditions; e.g., Austrheim, 1987; Rubie, 1986; Wayte et al., 1989). Fluids are known to play a major role in enhancing reaction rates (Pattison et al., 2011; Rubie, 1986). It is relatively difficult to assess the validity of the equilibrium versus disequilibrium hypotheses in fluid-undersaturated environments (see Putnis, 2021, for a thorough discussion), as reaction kinetics cannot be quantified easily based on natural samples. Moreover, estimating H_2O activity is difficult due to restricted equilibrium domains in dry rocks. Preliminary experiments designed at quantifying this effect have validated this inference (Joachim et al., 2019; Kemmert et al., 2017), although we are still far from a complete view due to the difficulty of experimentally controlling H_2O activity during metamorphic transformations.

However, the effects of H_2O on the mechanical properties of rocks and on rheology has received only limited attention in the metamorphic petrology community. Rybacki and Dresen (2004) have shown, based on laboratory experiments, that the presence of H_2O in trace amounts in feldspar aggregates dramatically affects the effective strength, with up to 2–3 orders of magnitude difference in strength compared to dry rocks. Feldspar is by far the most abundant mineral constituent of the middle and lower crust (Deer et al., 2013) and it is commonly accompanied by either stronger (e. g., garnet) or weaker (e. g., mica, quartz)

phases. Therefore, variations in the H_2O content, as well as the bulk mineralogy, can lead to effective strength contrasts that could affect the stress field and result in locally marked mechanical response to stress, such as localized deformation, formation of shear zones, or even the development of heterogeneous *P*. However, the effect of strength variations caused by gradients in H_2O content has not been investigated. Therefore, in this contribution, we explore the role of fluids on the deformation and metamorphic record in a polymetamorphic unit of the Western Alps that underwent eclogite-facies conditions during Alpine orogeny. Based on petrological arguments and thermodynamic as well as thermo-mechanical numerical modelling, we suggest that H_2O-undersaturated rocks may have been sufficiently strong to remain undeformed and develop large differential stress associated with a lower peak *P* during Alpine orogeny.

Geological setting

The Gran Paradiso Nappe

The Gran Paradiso Nappe belongs to the Internal Crystalline Massifs, together with the Monte Rosa and the Dora Maira nappes (e.g., Le Bayon, 2005). It corresponds to the middle Penninic Unit of the Western Alps (Fig. 1a) and was part of the former European-derived Briançonnais microcontinent, a ribbon of continental crust lying between the European and Adriatic plates (Michard et al., 2022). During Alpine orogeny, the closure of the Piemonte-Liguria oceanic domain was followed by the subduction of the Briançonnais microcontinent, leading to the formation of a tectonic nappe that was successively backfolded and exhumed along with the Penninic nappe stack (Le Bayon and Ballèvre, 2006; Manzotti et al., 2018).

The Gran Paradiso Nappe consists of a polymetamorphic Variscan basement, made up of paragneisses and micaschists, that locally contain amphibolite boudins (Fig. 1b; Biino and

Pognante, 1989; Compagnoni et al., 1974; Compagnoni and Prato, 1969; Manzotti et al., 2014). The basement metasediments were intruded by porphyritic granitoids in the Late Paleozoic, dated at 277 to 264 Ma by U/Pb on zircon (Bertrand et al., 2006; Ring et al., 2005). They are now mostly outcropping as undeformed metagranites to strongly foliated augen-gneisses (Le Bayon and Ballèvre, 2006).

Tectono-metamorphic evolution

The metamorphic evolution of the nappe is characterized by a first equilibration under amphibolite-facies conditions during the Variscan orogeny, estimated at 0-5-0.9 GPa and 600-650 °C (Gasco et al., 2010; Le Bayon et al., 2006), based on the chemical composition of pre-Alpine garnets in polymetamorphic paragneisses. Evidence of this metamorphic event is scarce and locally restricted to the presence of relict garnet porphyroclasts and the preservation of low-pressure, high-temperature accessory minerals, such as ilmenite, in inclusions in garnet. The intrusion of granitic bodies in the Late Palaeozoic lead to the formation of a thin contact aureole in the paragneiss surrounding the granites, which resulted in the development of hornfelses at conditions of 0.25 to 0.35 GPa and 670-700 °C (Gabudianu Radulescu et al., 2011). Locally, pegmatites have been observed, that crosscut the pre-Alpine, Variscan foliation (Le Bayon, 2005). The pre-Alpine foliation associated with the Variscan orogeny is mainly recorded in the low-strain areas of the nappe, whereas it is overprinted by the younger deformation and Alpine metamorphic mineral assemblages in most places throughout the nappe (Le Bayon, 2005; Le Bayon and Ballèvre, 2006).

Alpine metamorphism in the Gran Paradiso nappe was extensively studied (Ballèvre, 1986; Borghi et al., 1996; Brouwer et al., 2002; Compagnoni and Lombardo, 1974; Compagnoni and Prato, 1969; Dal Piaz and Lombardo, 1986; Gabudianu Radulescu et al., 2011; Gasco et al., 2010; Le Bayon et al., 2006; Manzotti et al., 2018, 2015; Massonne, 2015) and estimates

of the peak Alpine *P* and *T* conditions vary between 1.4 – 2.7 GPa and 490 – 600 °C, depending on the studies. The Alpine peak stage was dated at 41.5 ± 0.3 Ma by in situ U-Th/Pb LA-ICP-MS technique on monazite by Manzotti et al. (2018). A H*P* deformation event was characterized, mainly based on structural data from mafic eclogites, that show a N-S stretching lineation (Le Bayon and Ballèvre, 2006). The whole nappe underwent a younger deformation event, coeval with an albite-epidote-amphibolite facies stage. This younger deformation phase is associated with nappe stacking, exhumation and backfolding. It almost pervasively affected the nappe and partially overprinted the high-pressure stage (Le Bayon and Ballèvre, 2006). The main foliation developed during this event defines the broad regional dome-shape of the nappe and is characterized by an E-W stretching lineation and a sub-horizontal foliation, moderately dipping to the north in the northern part of the nappe, with top to the west sense of shear (Le Bayon and Ballèvre, 2006).

Field observations

The studied area is located in the Valeille valley, in the northern part of the Gran Paradiso massif, south of the Aosta valley in north-western Italy. There, previous glaciation events deeply dug the valley along a N-S orientation. On both sides of the valley, a large body (ca. 200 m x 100 m) of Alpine low strain paragneisses crops out, surrounded by Alpine high strain paragneisses (Le Bayon, 2005; Le Bayon and Ballèvre, 2006). The Alpine low strain body is delimited in the South by a sub-vertical shear zone and in the North by a northward dipping foliation (Fig. 2a). The foliation in the North and South wraps around the low strain paragneisses. Both are essentially parallel and belong to the same deformation event. The overall shape of the Alpine low strain paragneisses mimics the shape of a boudin, with the swell region on the bottom of the valley and the necking zone on the top (Fig. 2b). The foliation within the Alpine low strain paragneisses is sub-horizontal. The prolongation of

these structures, i.e., the shear zone and northward dipping foliation, including the Alpine low strain volume, are also visible in the Bardoney valley, on the East of the Valeille. Both volumes of low strain paragneisses were interpreted by Le Bayon and Ballèvre (2006) as a unique volume, cropping out laterally in the two valleys and delimited by the same shear zone. In the Bardoney valley, undeformed pre-Alpine pegmatites crosscut the sub-horizontal foliation, attesting for the pre-Alpine age of the foliation within the Alpine low strain body. Eclogitic boudins are also found, embedded within the paragneiss of the sub-vertical Alpine shear zone, that preserved the Alpine high-pressure foliation, hence indicating that the activity of the shear zone had already started during the high pressure history (Le Bayon and Ballèvre, 2006). The structural data that support this interpretation can be found in Le Bayon and Ballèvre (2006) as well as in Le Bayon (2005), along with petrographic argument that support eclogite facies conditions for the mafic rocks. Two samples from the Valeille valley were selected for detailed investigation. Sample 20GP10 was collected in the Alpine shear zone, South of the Alpine low strain paragneiss and sample 20GP07 was collected in the Alpine low strain paragneiss body (Fig. 2b).

Methods

Optical microscopy and electron probe microanalysis (EPMA)

Thin sections were studied using optical microscopy and back-scattered electron microscopy prior to quantitative analysis by electron probe microanalysis (EPMA). Mineral spot analyses and X-ray element maps were performed using a Cameca SX100 electron microprobe at the Microsonde Ouest facility in Brest, France. 1 µm spot analyses of garnet and 3 µm spots analyses of plagioclase were acquired with operating conditions set to 15 kV, 20 nA and 10 s counting time on the peak, except for Ti, 30 s. Standards used are natural minerals:

Journal Pre-proof

wollastonite (Si, Ca), corundum (Al), andradite (Fe), forsterite (Mg), $MnTiO_3$ (Mn, Ti), albite (Na), orthoclase (K), apatite (P), and Cr_2O_3 (Cr). 5 µm spot analyses of mica and chlorite were acquired with operating conditions set to 15 kV, 20 nA and 10 s counting time on the peak, except for Ti and F, 30 s. Standards used are natural minerals: wollastonite (Si, Ca), corundum (Al), andradite (Fe), forsterite (Mg), $MnTiO_3$ (Mn, Ti), albite (Na), orthoclase (K), apatite (F), and pyromorphite (Cl). Structural formulae were calculated based on 8 cations for garnet, 11 oxygens for mica, 8 oxygens for feldspar and 23 oxygens for amphibole. The X_{Mg} is calculated as the ionic ratio of Mg/(Mg+Fe) in mica and X_{An} is calculated as Ca/(Ca+Na) in plagioclase. Mineral abbreviations follow the system of Warr (2021).

Thermodynamic modelling

Equilibrium phase diagrams were calculated using the software suite Theriak-Domino (de Capitani and Brown, 1987). *P-T* pseudosections for sample 20GP10 were calculated using the 6.2 dataset of Holland and Powell (2011) and the following solution models: garnet, phengite, biotite, chlorite, chloritoid, staurolite, and ilmenite (White et al., 2014); clinoamphibole, clinopyroxene (Green et al., 2016); epidote (Holland and Powell, 2011); and feldspar (Baldwin et al., 2005). The reactive bulk composition of both samples was calculated by combining mineral compositions with the modal amounts (in %) of phases from a selected area, determined based on image analysis of the grey-scale levels of the backscattered electron images. Garnet cores interpreted as pre-Alpine (2 vol%; see below) were removed from the reactive bulk composition. H_2O-saturated conditions were assumed. The reactive bulk composition of the shear zone sample 20GP10 used for calculations is the following (in moles): Si(58.75), Ti(0.87), Al(20.43), Fe(5.94), Mn(0.16), Mg(3.85), Na(1.87), Ca(2.51), K(5.63), H(30).

Journal Pre-proof

A *P–T* diagram showing the colormap and isopleths of total H_2O content of solids (in mol%) was drawn for the pre-Alpine paragneiss, sample 20GP07. Given that these rocks were neither deformed nor totally transformed during Alpine orogeny (see below), it is difficult to assess the area to take into account for a reactive bulk composition estimate. However, slight changes in the reactive bulk composition do not significantly affect the general trend shown by the results and hence we use the reactive bulk composition of sample 20GP07 of (in moles): Si(62.27), Al(20.34), Fe(4.48), Mg(3.08), Na(4.10), Ca(0.72), K(4.77), H(30).

Thermo-mechanical modelling

The numerical models were designed using the 2D thermo-mechanical code MDoodz (Duretz et al., 2021). The code is based on the finite difference method/marker-in-cell approach and allows studying large strain deformation of heterogenous materials. A rectangular model domain of 2 × 1 km was designed, consisting of a homogeneous matrix with an oblique layer in the center, to study the effects of shearing on a competent dry rock layer embedded in a weaker hydrated rock matrix. The rheological model is visco-elasto-plastic and material parameters are based on rock deformation data. In order to investigate the effect of H_2O on the viscous rheology of the matrix and layer, we prescribed laboratory-derived flow laws of anorthite wet (An100, 0.07 wt% H_2O; Rybacki and Dresen, 2000) and anorthite dry (An100, 0.004 wt% H_2O; Rybacki and Dresen, 2000) in the matrix and layer respectively. The plagioclase viscous flow laws were used, because they are representative of crustal rocks and these laws were derived consistently for different H_2O contents, which is precisely the parameter of interest of this study. The plastic rheological model is frictional and is based on the Drucker-Prager model. An initial background *P* of 1.6 GPa is applied. The model setup consists of a 2×1 km wide box, containing a strong layer inside a weak matrix. The strong layer has an initial angle of 85° from horizontal direction. Top to the right shear deformation

is applied at the top and bottom boundaries inducing a bulk strain rate of 10^{-14} s^{-1}. Periodic boundary conditions are applied to the lateral sides. Flow laws of dry (0.004 wt% H_2O) and wet feldspar (0.07 wt% H_2O) are attributed to the strong and weak materials, respectively (Rybacki and Dresen, 2000). A seed with the similar properties as the matrix (weak hydrated) is placed in the middle of the competent layer. This heterogeneity induces a stress perturbation, which promotes necking in the middle domain rather than along the top and bottom boundaries. The model parameters are summarized in Table 3.

Results

Petrography, structures and mineral chemistry

Shear zone paragneiss 20GP10

Sample 20GP10 is a polymetamorphic schistose garnet metagrauwacke (Fig. 3a). It consists of a fine-grained assemblage of garnet (18 vol%), phengite (35%), plagioclase (10%), quartz (25%), biotite (5%), chlorite (3%), titanite (2%), epidote (1%) and minor amounts of the accessory minerals rutile, ilmenite, apatite and zircon (together 1%). The foliation is spaced, with mica-chlorite rich layers separating quartzofeldspathic rich layers (Fig. 3). The foliation can be characterized as a disjunctive foliation, according to the nomenclature of Passchier and Trouw (2005, p. 78). In the quartzofeldspathic layers, micas are aligned obliquely to the mica-chlorite layers. The latter form the cleavage layers and are parallel. The spacing occurs over a millimeter scale distance and is hence better visible at the thin section scale. In the quartzofeldspathic layers, the foliation is essentially defined by white mica and elongated quartz aggregates, which wrap around garnet porphyroblasts. Garnets occur either as few large subhedral porphyroblasts (up to 800 µm in size), or mostly as small subhedral to euhedral garnets (50 – 100 µm in size). Pre-Alpine, supposedly Variscan (see Nosenzo et al.,

2022 for a discussion on pre-Alpine garnet ages) garnet cores (Grt_V) are often found both within the Alpine large and small garnets. Grt_V are identifiable in thin section because they are usually rimmed by early Alpine garnets (Grt_A) that are rich in inclusion, with mostly rutile. In some Grt_A, small rutile inclusion trails also follow the schistosity. The transition between the Grt_V and the Grt_A is irregular, suggesting that the Grt_V were resorbed before the growth of Grt_A. Apatite, zircon and ilmenite are other relic minerals from the Variscan stage, that were not completely resorbed. The irregular external outline of most garnets suggests partial resorption on a late stage as well. Garnet is also fractured, and the fractures are mostly filled with chlorite. Rutile is found either as inclusion within garnet and plagioclase, or in the matrix. Two types of plagioclases were observed. The first one consists of poikiloblastic plagioclase riddled with inclusions of garnet, phengite, rutile, and quartz. The schistosity defined by phengite is preserved in the plagioclase, indicating that plagioclase grew during the Alpine history, and is post-kinematic with respect to the earlier Alpine deformation. The second consists of equant, often elongated euhedral plagioclase, found in aggregates with chlorite and quartz, suggesting that they could represent breakdown products of glaucophane. Biotite is an Alpine post-kinematic phase, growing at the expense of white mica, mainly at its extremities, or where it is in contact with garnet (Fig. 3b). Titanite is mainly found as rims overgrowing rutile in the matrix. In the quartzofeldspathic rich layers, chlorite is the youngest post-kinematic phase, found either as large individual crystals in the plagioclase-chlorite-quartz aggregates, or as minor amounts of very fine-grained crystals replacing biotite and phengite. Chlorite in the mica-chlorite rich domains is parallel to the foliation, suggesting that the deformation was probably continuous from the Alpine peak conditions (at H*P*) to greenschist-facies conditions.

Large garnet porphyroblasts have cores of the Grt_V generation, hence an area devoid of those large garnets was selected as a representative area in order to estimate the reactive bulk

composition and conduct quantitative phase petrology analysis. Among the small subhedral garnets, a few of them show cores of pre-Alpine Grt_V, that are identifiable by their chemical composition, with in particular low Ca content (5 to 7 mol% grossular) and high Mn content (up to 32 mol% spessartine; Fig. 4a and e). Alpine Grt_A display an irregular growth zoning, with first an increase in Ca (grossular content up to 28 mol% - locally up to 32 mol%), and a subsequent decrease to 15 mol% (Fig. 4b), which is compensated by a first decrease in almandine content to 60 mol% and then an increase to 68 mol% towards the rim (Fig. 4c). Pyrope content in Grt_A is rather constant in the core (Fig. 4d and f), with 7.8 to 8.0 mol%, and slightly increases up to 12 mol% towards the rim (Fig. 4f). Spessartine content in Grt_A is 3 mol% and increases to 6-8 mol% towards the rim. Based on the zoning characteristics, an Alpine peak composition can be deduced, with 28 - 32 mol% grossular, 7.8 to 8.0 mol.% pyrope, 60 mol% almandine and 3 mol% spessartine.

White micas are zoned and their chemical composition corresponds to the phengite series (Supplementary Material S3). They show aluminum contents that are lower in the cores than in the rims (Fig. 5a). Silicon contents range between 3.25 to 3.53 atoms per formula unit (a.p.f.u), with one outlier at 3.16 a.p.f.u. The trend in silicon content correlates with the Tschermak exchange vector (Fig. 5b). The increase in silicon content is also correlated with a decrease in titanium (Fig. 5d). No relics of pre-Alpine, low-Si compositions have been found in this sample.

Chlorite can be separated into two groups, based on their chemistry. The large individual crystals found in aggregates with plagioclase and quartz are magnesium-rich (X_{Mg} = 0.56) and small crystals in the matrix and in the fractures of garnet are magnesium-poor (X_{Mg} = 0.35). The EPMA data confirmed the presence of two types of feldspars: poikiloblastic feldspars are nearly pure albite in composition (X_{an} = 0.00 to 0.05), whereas feldspars in the chlorite-quartz-feldspar aggregates have a X_{an} ranging from 0.29 to 0.33.

Journal Pre-proof

Low Alpine strain paragneiss 20GP07

Sample 20GP07 is a foliated paragneiss, consisting of white mica (35%), plagioclase pseudomorphs (17%), quartz (30%), biotite (3%), garnet (10%), chlorite (5%) and amphibole (~ 1%). Accessory minerals are clinozoisite, tourmaline, apatite, zircon, titanite, ilmenite and rutile. The foliation is defined by alternating quartz and white mica layers, wrapping around plagioclase porphyroblasts. White micas (hereafter all called phengite whatever their silica content, according to the classification of Rieder et al., 1998) appear mainly as elongated coarse-grained phengite flakes, which are oriented parallel to the foliation, or set in randomly oriented packages (Fig. 3c). As the coarse-grained phengites define the foliation of the sample, they are interpreted as belonging to the pre-Alpine, Variscan generation (Ph_V). A younger, Alpine generation of phengite is characterized by randomly oriented, fine-grained phengite crystals (Ph_A), found locally in association with garnet, rutile, ilmenite, amphibole, ± quartz, or as overgrowth on Ph_V. Garnets are small subhedral crystals (20 – 100 µm) and usually found in clusters, associated with fine-grained phengite (± biotite, chlorite, amphibole, ilmenite, rutile) between Ph_V and the former plagioclase domains (Fig. 3d). The inclusions in garnet are mostly rutile. The plagioclase domains consist of an assemblage of albite and very fine-grained phengite, clinozoisite and chlorite. Biotite is found as a late replacement of Ph_A, as replacement of phengites that are in contact with garnet, or as individual small crystals in the plagioclase domains. Indication of the presence of pre-Alpine biotite that has been pseudomorphosed is seen in areas where Ph_A flakes are included with sagenite needles. These Ph_A are usually also partially rimmed with garnet. Chlorite is found essentially in the plagioclase pseudomorphs, as individual crystals, or as replacement of biotite. A few amphibole grains were found, in association with the clusters of fine-grained Ph_A, garnet, biotite and chlorite. They show a brownish-green pleochroism, similar to the one

of biotite and can only be confidently distinguished from biotite based on the extinction angle. Amphibole occurs as small individual crystals, in very low modal amounts (ca. 1 vol%) and there is no textural indication that could suggest that it replaces former glaucophane.

The overall microtextures as well as the evidence that the foliation is pre-Alpine show that the rock was neither completely transformed, nor deformed during Alpine orogeny. This is also supported by the large chemical range of phengite (Fig. 5c), with high aluminum Ph_V (up to 0.05 a.p.f.u.) and low aluminum Ph_A (0.01-0.02 Al a.p.f.u.). The correlation between silicon content and the Tschermack exchange vector forms a continuous compositional trend from 3.05 to 3.49 Si a.p.f.u (Fig. 5b). The high titanium content of the low-silicon Ph_V suggests a formation under high-temperature conditions (Auzanneau et al., 2010), which is another argument in favor of a Variscan age for the Ph_V generation. Finer-grained randomly-oriented phengite clusters surrounding coarse-grained phengites also have high Al cores, similar to the coarse-grained Ph_V and are therefore also interpreted as Variscan. Garnets show irregular growth zoning. Most garnet cores are almandine rich (70 – 76 mol%), grossular poor (1 – 10 mol%), have low pyrope contents (10 – 20 mol%) and variable spessartine content (3 – 15 mol%). A decrease in almandine (60 – 70 mol%), and pyrope (6 – 16 mol%) as well as an increase in grossular content (10 – 23 mol%) is often observed towards the garnet rims, whereas spessartine content is variable and does not show a spatial trend. Overall, the zonation patterns are usually neither regular nor symmetric, as shown by the variable spessartine content. Plagioclase is mostly albitic in composition, with X_{an} ranging from 0.00 to 0.07. A few outliers have X_{an} of 0.19 to 0.23. The amphibole compositions correspond to the sodic-calcic group, and more specifically match the compositional range of barroisite.

Journal Pre-proof

***P-T* estimates**

Alpine peak *P–T* estimates were undertaken on sample 20GP10 using phase equilibria modelling. This method could not be applied to sample 20GP07 due to the too large disequilibrium. Hence, only an estimate of the maximum value of the peak *P* will be assessed based on its mineralogy and assuming a temperature of 500-520 °C, as determined for the peak conditions of sample 20GP10.

Sample 20GP10

The *P–T* pseudosection was calculated in the system MnNCKFMASHT for a reactive bulk composition including the mapped area of Fig. 4 (see methods for details). The isopleths of pyrope and grossular mole fractions in garnet have been calculated and compared to the composition of the garnets in order to constrain the peak *P-T* conditions (Fig. 6). The isopleths of pyrope and grossular crosscut in the stability field of garnet, phengite, glaucophane, chloritoid, lawsonite, quartz and rutile, with peak *P – T* conditions inferred at 1.80 – 1.95 GPa and 500 – 520 °C. Note that the silica in phengite barometer of Massonne and Schreyer (1987) cannot be applied to this rock because it lacks the buffering assemblage K-feldspar, biotite and quartz at the peak conditions. The modelled mineral mode corresponds to the observed mode for garnet (11%, taking into account only the vol% of the observed Alpine garnet cores) and quartz (28%). Phengite is slightly overestimated in the calculations (42%, in comparison with 35% observed), however part of the potassium attributed to phengite would be compensated by biotite growth upon decompression, which explains such high values for the modelled amount of phengite. According to the pseudosection of Fig. 6, the H*P* sodic phase is glaucophane (11 vol%). Although glaucophane is not observed in the mineral assemblage, its former presence is suggested by the occurrence of Mg-rich chlorite, plagioclase and quartz aggregates. Lawsonite and chloritoid have not

been identified in the sample, however their calculated modal abundances are 4 and 1 vol%, respectively. Both phases could account for the Ca and Mg-Fe contained in the plagioclase and chlorite now occurring as retrograde phases. They could have been dissolved during the post-peak retrogression during the late stages of deformation associated with the activity of the shear zone. Chlorite and biotite are late phases and are interpreted as not being part of the peak assemblage. The stability field of chlorite reaches relatively high *P* at *T* of 500 to 520 °C and the biotite breakdown reaction is reached at *P* of 1.3 – 1.4 GPa over this temperature range. The absence of both phases from the peak assemblage hence supports the estimated high value of *P*. Moreover, the *P–T* conditions estimated agree with estimates from the literature for similar rock types in the northern part of the Gran Paradiso Unit (Le Bayon et al., 2006; Manzotti et al., 2015, 2018).

Sample 20GP07

Due to the large apparent disequilibrium over the mm scale, as shown by microtextural/microchemical observations, the preservation of pre-Alpine mineral phases (such as the white mica Ph_V), as well as the large compositional range of phengite, a paleo-equilibrium domain could not be reliably defined. Garnet zonation is not regular, with intra- and inter-grain chemical innomogeneities, so they cannot be used to determine the Alpine peak *P* composition. Moreover, the isopleths of the silicon in phengite are sub-vertical in the pressure and temperature range of interest, which does not provide a reliable pressure indication (see Supplementary Material, Fig. S1). Therefore, phase equilibrium modelling cannot be applied reliably to this rock. However, an attempt to determine the peak *P* range can be made, based on petrographic observations. First, it is important to note here that thermodynamic disequilibrium at the thin section scale does not imply a lack of reaction at the grain scale. It is evident that the rock has been partially affected by Alpine

metamorphism, as attested by the occurrence of high silica phengite, garnet and rutile. Along with barroisite, plagioclase is the only sodium-bearing phase present in the rock. The stability limit of plagioclase is expected to end at *P* around 1.4 GPa for temperature of 500 to 520 °C (Holland, 1980). Above that *P*, the expected stable sodium-bearing phases are paragonite, glaucophane and sodic pyroxene. However, paragonite, glaucophane, or sodic pyroxene are not observed in the sample, neither were any indications of their former presence found. Barroisite occurs as a minor phase, representing ca. 1 vol% of the sample, and is observed as dispersed crystals. It does not occur as pseudomorph after glaucophane, neither as a reaction rim around former glaucophane, despite the absence of deformation. Moreover, it is found in association with Alpine garnet and phengite in the plagioclase domains and hence, it seems to be stable along with plagioclase.

With respect to plagioclase, the reaction history within sample 20GP10 may have followed different paths.

1. The pre-Alpine plagioclase may have remained metastable at peak *P-T* conditions, and may have been transformed into an albite-bearing aggregate during decompression. This hypothesis would be consistent with the lack of jadeite, or products of replacement of jadeite (provided we are able to identify them). Metastability of plagioclase would have been favored by the lack of strain energy (this sample is in the undeformed volume) associated to the lack of additional H_2O entering the system and allowing the growth of a Ca-bearing, hydrated, phase (zoïsite) necessary to account for the anorthite component.
2. The pre-Alpine plagioclase may have been replaced by albite and zoisite during the late-Variscan history, or during the prograde Alpine history. In such a hypothesis, albite was still stable at peak *P-T* conditions in the undeformed volume, thus limiting the peak *P* range for sample 20GP07 to a maximum value of 1.4 GPa.

Journal Pre-proof

3. Last, the pre-Alpine plagioclase may have been replaced by a fine -grained aggregate consisting of jadeite and zoïsite, as described in some H*P* metagranites (for a recent summary, see Schorn, 2022), later replaced by albite during decompression. We lack unambiguous textural and mineralogical evidence in favor of this hypothesis.

In the light of the results presented for the two samples, there are two points in which the samples differ strikingly. First, from a petrological perspective, sample 20GP10 equilibrated to the evolving *P*-*T* conditions during the Alpine orogeny, whereas in sample 20GP07 a large proportion of the low *P* pre-Alpine minerals were preserved during Alpine orogeny. Second, from a structural perspective, the sample 20GP10 was pervasively deformed during the formation of the shear zone, whereas the sample 20GP07 remained mostly unaffected by Alpine deformation. There is hence an apparent relationship between the extent of deformation and the extent of Alpine metamorphic equilibration between the two samples, suggesting that in this case, fluids played a major role in the establishment of the structural and petrological characteristics of the samples.

Discussion

Geological significance

Based on our results, there is a discordance in apparent peak *P* between the sample 20GP07 (*P* <1.4 GPa, according to hypothesis 2 above) and the shear zone paragneiss 20GP10 (ca. 1.8 –1.9 GPa) of at least 0.4 GPa. Compared to the previous peak *P* estimates for the Gran Paradiso nappe, both peak *P* fit into the estimated range from the literature (from 1.2 to 2.7 GPa, see introduction). Although the geothermobarometric methods have constantly evolved (Lanari et al., 2019) since the first Alpine peak *P* estimates in the Gran Paradiso by Dal Piaz and Lombardo (1986), it is unlikely that the methodology can solely explain the discrepancy

Journal Pre-proof

in peak *P*. It is therefore evident that we are facing a problem, which relates to the interpretation of such *P* variation at the outcrop scale. Here, the rocks that did record the highest peak *P* are also the rocks that are deformed and, in the opposite, the rocks that seem to record a large thermodynamic disequilibrium are the least deformed. The relationships between deformation and metamorphism are usually tightly related to the conditions of access to fluids and fluid-rock interactions (e.g., Rubie, 1986). In the next section, we discuss independently the role of H_2O on the progress of metamorphic reactions and on the mechanical behavior of rocks under stress.

The role of H_2O in metamorphism

Fluids involved in subduction and continental collision settings at the pressures and temperatures considered in this study are likely aqueous solutions, essentially made of H_2O in the form of supercritical vapor. Minor constituents, such as CO_2, N_2 and ions in solution may be found as well (e.g., Ferry and Burt, 1982), but for simplicity we will generalize the nature of fluids to pure H_2O in the following discussion. H_2O is found under different forms in rocks (see Putnis, 2021, for a review). In non-deforming fluid saturated rocks, hydrous species are present in the grain boundary region, either in isolated pores or as interconnected fluid-filled porosity, so that at equilibrium the fluid pressure equals the total pressure. In fluid undersaturated rocks, either aqueous species are present in the grain boundary region in the form of isolated H_2O molecules, or dissolved OH^- and H^+, forming disconnected fluid films and then the rock is nearly anhydrous. The latter situation is often found in high-grade rocks, such as granulites, in which not even hydrous minerals are stable. Note that nominally anhydrous minerals can also contain H_2O in the form of structurally bonded hydrogen or fluid inclusions. The H_2O saturation conditions are susceptible to evolve through time, especially

during metamorphism, with for example dehydration reactions, or fluid infiltration events (Thompson, 1983).

Even if H_2O does not participate to metamorphic reactions as a thermodynamic component, its presence in the grain boundary region has a significant catalytic effect on reactions (e. g., Rubie, 1986; Wayte et al., 1989). H_2O acts as a transport medium, in which ions migrate by diffusion from the reactant site to the product site. Reaction rates are enhanced by several orders of magnitude in the presence of a free intergranular fluid (Carlson, 2010; Rubie, 1986). Under H_2O undersaturated conditions and at *T* such as those estimated here, timescales for intergranular diffusion of most ions are longer that the geological timescales under interest (Ahrens and Schubert, 1975). The kinetics of metamorphic reactions in dry rocks is therefore expected to be very slow, thus limiting the extent of reaction product formation or even prohibiting the formation of the expected paragenesis at high *P* conditions, which leads to the occurrence of mineral assemblages, that are outside of their stability field as long as there is no deformation or fluid input (Rubie, 1998). Many examples from tectonic units where portions recorded lower peak *P* than the neighboring rocks are interpreted as metastable based on the apparent lack of reaction products. However, according to experiments of reaction rim growth, the minimum amount of H_2O necessary to qualify a system as "hydrous" is very low, in the order of a few tens of ppm of H_2O (Milke et al., 2013). Beyond this threshold, even minute amount of H_2O is sufficient to trigger metamorphic reactions under geologically realistic timescales. Hence, totally inhibited reactions in presumably metastable rocks imply extremely dry conditions.

Reaction pathways in the Gran Paradiso samples

Timing and degree of equilibration in the shear zone sample 20GP10

Journal Pre-proof

The deformed paragneiss 20GP10 has been almost completely equilibrated during the Alpine orogeny, with garnet cores Grt_V being the only remnants of the former Variscan amphibolite-facies mineral assemblage (excluding other relict accessory minerals). Grt_V cores occur everywhere in the sample. They are highly resorbed, suggesting that the rock was almost pervasively altered by fluids after the Variscan orogeny and before the Alpine peak *P* event. Garnet probably acted as a refractory mineral during this alteration event. One hypothetical scenario that could explain the partial resorption of the garnet could be that the paragneisses from this location were affected by an external fluid infiltration before Alpine orogeny. Such fluid-rock interaction could have occurred very locally, along with a deformation event (e.g., a fault zone), which would have acted as a structural heterogeneity and would have preferentially enhanced further ductile strain localization during Alpine deformation. In this case, local external fluid infiltration would have occurred only in the vicinity of the shear zone and would not have affected the low strain paragneiss. This interpretation is supported by the observation that Variscan minerals are preserved in the low-strain paragneiss and only locally re-equilibrated under Alpine HP conditions.

Microstructural observations in sample 20GP10 show that the Alpine deformation related to the formation of the shear zone precedes the growth of albite poikiloblasts, biotite and chlorite. Therefore, it is inferred to have occurred at H*P* conditions. The schistosity defined by high-silica phengite also supports this interpretation. Overall, the petrographic and microtextural observations suggest that the prograde to peak metamorphism occurred under fluid saturated conditions. Therefore, the use of fluid saturated conditions for pseudosection modelling seems justified, as prograde increase in *P* and *T* conditions would essentially lead to dehydration and further fluid supply. Then, fluids must have been available sporadically during the retrograde part of the metamorphic history, in order to provide the H_2O necessary to form the low-silica phengite rims as well as the late chlorite.

Timing and degree of disequilibrium in the low strain paragneiss 20GP07.

The observation of extensive disequilibrium textures in the low-strain paragneiss 20GP07 would indicate that thermodynamic equilibrium was not reached at the sample scale, or even at the grain scale, during the Alpine orogeny. Such interpretation involving sluggish kinetics has already been invoked to explain the apparent lack of reaction and significant pressure overstepping in various metamorphic rocks in the Alps and worldwide (e. g., Austrheim and Griffin, 1985; Proyer, 2003). Proyer (2003) as well as Schorn (2018) discuss the role of H_2O on the preservation of mineral assemblages during prograde and retrograde metamorphic conditions. In particular, Proyer (2003) shows, based on phase equilibria modelling, that orthogneisses require a significant amount of H_2O addition from external sources on the prograde path in order to equilibrate to high pressure conditions. In order to test the applicability of this scenario to the Gran Paradiso low-strain paragneiss, a *P–T* pseudosection showing the H_2O content (in mol%) of the mineral assemblage was calculated, based on the reactive bulk composition of sample 20GP07 (Fig. 7). The peak *P–T* conditions of the shear zone paragneiss 20GP10 are represented with the red star, as well as the corresponding prograde *P-T* path, according to Le Bayon et al. (2006). Three grey arrows show typical geothermal gradients for subduction zone environments (6, 10 and 15 °/km). The black dashed line shows the position of the albite breakdown reactions: albite = jadeite + quartz (Holland, 1980). The blue star at 600 °C and 0.5 GPa indicates the *P–T* conditions inferred for the pre-Alpine amphibolite facies conditions reached by the Gran Paradiso basement rocks (Le Bayon et al., 2006). The white dashed lines represent the total H_2O content in the mineral assemblage, in mol% (meaning the sum of all H_2O content in mineral phases – without adding a fluid phase in an unspecified porosity). The H_2O content isopleths have a positive slope in the P-T diagram, with an increasing amount towards higher *P* and lower *T*.

The isopleths on Fig. 7 show that under normal prograde increase in *P* and *T* along either of the geothermal gradients, the total H_2O content decreases, hence the rock should dehydrate. Metamorphic reactions under such conditions are normally favored, since H_2O is progressively being released and can hence contribute to the catalysis of metamorphic reactions. However, this is true for a rock, whose protolith has a high initial H_2O content (i.e., above ca. 8 mol%, corresponding to the H_2O content at similar peak conditions as the shear zone paragneiss; red star on Fig. 7), such as marine sedimentary rocks saturated in H_2O during their deposition, and constantly evolving across/through dehydration reactions.

In the case of a polymetamorphic rock, such as sample 20GP07, the H_2O content of the rock before Alpine metamorphism may be the one acquired at amphibolite facies conditions, during the pre-Alpine Variscan metamorphism. In this case, the paragneiss has a H_2O content of ca. 5.7 mol% (blue star on Fig. 7). Even if the sample has been affected by retrograde hydration after Variscan amphibolite facies during its cooling history, it would only result in a final H_2O content < 6 mol%, according to the H_2O isopleths for a constant *P* of 0.5 GPa. Therefore, a fluid input from an external source is required in order to allow for equilibration of the mineral assemblage at *P*–*T* conditions higher than those allowed at the corresponding total H_2O content. If no external fluid is added to the rock, it will remain untransformed during a prograde increase in ambient *P* and *T* conditions. In such a case, the persistence of low *P* parageneses are not necessarily attributed to metastability, as long as fluid-absent reactions are not overtaken, because the stability limits in terms of *P* and *T* of a H_2O-free assemblage delimit a greater field than for the same rock with free H_2O. Nevertheless, crossing the albite breakdown reaction without producing jadeite and quartz because of a lack of catalytic H_2O would lead to metastability. In the case of 20GP07, glaucophane would be expected to form at the peak conditions inferred for the shear zone paragneiss 20GP10. The lack of a H*P* sodic phase in the rock could then suggest that the rock persisted to metastable

conditions at high *P–T* conditions. However, this interpretation is not unique. Although this is not straightforward at the first sight, there are examples in the literature demonstrating that apparent disequilibrium textures, such as zoned reaction rims or orientation dependent reaction products can be explained by equilibrium processes in systems under high differential stress (e.g., Cionoiu et al., 2019; Tajčmanová et al., 2014). Therefore, the metastable state of a rock cannot be inferred purely based on phase equilibria considerations, and the effect of the stress state on mineral compositions is similarly important, and must not be overlooked (Tajčmanová et al., 2015).

In the framework of our study, an alternative mechanism to metastability may be considered, that could explain the discrepant peak *P* record between samples 20GP10 and 20GP07. This interpretation, investigated below, involves a mechanical analysis of strength contrasts between hydrous and H_2O undersaturated rocks, that would produce a heterogeneous stress field during deformation, leading to local pressure variations. Here, we refer to hydrous rocks for rocks with a free fluid phase.

The role of H_2O on stress and pressure

Although the slow diffusion rates in H_2O undersaturated rocks are not put into question here, an alternative interpretation of the lack of reaction and deformation of the Gran Paradiso dry rocks in our case could be that dry rocks are stronger and the mechanical behavior would lead to the generation of tectonic under-pressure. The generation of heterogeneous stress conditions in inclusion - host systems has been shown by Moulas et al. (2014) to be a valid explanation for pressure variations. The analytical solution derived by Moulas et al. (2014) has later been applied to the high pressure whiteschists of the Monte Rosa nappe (Luisier et al., 2019a) and to an eclogite facies shear zone in the Bergen Arcs in western Norway (Jamtveit et al., 2018). Both studies use a rheological contrast between a strong host rock and

Journal Pre-proof

a weak inclusion and depending on the orientation and aspect ratio of the weak inclusions, pressure locally rises. The difference in pressure is explained by the force balance between a strong material which has a large differential stress and a weak material that has a small differential stress (see Fig. 4a in Jamtveit et al., 2018 for an explanation on the stress state).

The maximum differential stress that rocks can sustain without breaking depends on several factors, such as temperature and strain rate. The H_2O content is also an important factor controlling the strength of rocks (see Wong et al., 2016, and references therein). From experiments, it is well established that increasing H_2O content in a material at constant confining pressure causes a decrease in the material strength in comparison to H_2O absent conditions. This weakening mechanism was attributed to the hydrolysis of O–Si–O bonds in quartz in the presence of traces of H_2O, and is termed " hydrolytic weakening" (Griggs, 1967). As an example, the difference in flow strength between dry and wet samples is up to a factor of 2.5 for quartz (Koch et al., 1989). Rybacki and Dresen (2000) determined flow laws for dry and wet feldspar aggregates, with total H_2O contents of 0.004 and 0.07 wt%, respectively (i.e., the total H_2O including molecular H_2O or hydroxyl, fluid inclusions as well as the H_2O in the sample porosity of less than 1%). They show that the hydrolytic weakening effect causes a strength decrease up to a factor of 3 (Rybacki et al., 2006; Rybacki and Dresen, 2000).

The effect of H_2O content in rocks on the rheology during deformation was tested by designing a regional scale deformation simulation using a thermo-mechanical numerical code (see method section for details). Fig. 8 shows the temporal evolution of the *P* field (GPa) and accumulated strain during ongoing shear deformation. The strong layer is sheared and a pinch and swell structure starts forming after ca. 1 Ma of deformation, leading to the formation of distinct boudins and necking zones after 1.8 Ma. With increasing strain, the matrix behaves in a visco-elastically while the dry strong layer behaves dominantly in a plastic manner, as

witnessed by the occurrence of shear bands. The pressure field is heterogeneous both in the matrix and in the strong layer, with overall higher *P* in the matrix (1.6 to 1.9 GPa) and lower *P* in the strong layer (0.8 to 1.4 GPa). The first order distribution of the *P* agrees well with previous results of numerical models (Mancktelow, 2008). The accumulated strain is the lowest in the boudins and highest in the necking zones, with additional fringes of high strain areas developing from the necking zone towards the boudin swells, progressively wrapping around the boudins. One of such areas is highlighted by a red square on Fig. 8. Notably, these high strain areas are associated to higher *P* in the matrix, and could therefore be interpreted as a representative numerical equivalent area to the natural study area, with high strain and high *P* paragneiss surrounding the low strain and low *P* paragneiss boudin (see Fig. 2b for a sketch of the field area). In the red square, the *P* in the high strain matrix is similar to the *P* recorded by the shear zone paragneiss 20GP10 (1.9 GPa).

The effect of strain rate and background *P* on the *P* field were assessed through a parametric study, with the main results plotted in Fig. 9. Strain rates of 10^{-15}, 10^{-14} and 10^{-13} s^{-1} were compared, along with background *P* of 1.4, 1.6 and 1.8 GPa. The strain rate has a strong impact on the structure development, with slower strain rates enhancing the formation of thick boudins with more homogeneous *P* distribution. Larger strain rates result in large *P* perturbations in the strong layer along with a more pronounced shear effect, resulting in thinner, more elongated boudins. Larger strain rates also increase the *P* contrast between the strong layer and the weak matrix. Additionally, a slow strain rate of 10^{-15} s^{-1} results in the formation of distinct boudins and necking zones after ca. 17 Ma, whereas at large strain rates of 10^{-13} s^{-1}, pinch and swell structures already form after ca. 200 ka. Therefore, a low to intermediate strain rate of 10^{-15} to 10^{-14} s^{-1} seems more appropriate compared to the burial and exhumation rates derived from combined microtextural, petrological and geochronological data in the Gran Paradiso Unit (see Manzotti et al., 2018 for a synthesis).

Journal Pre-proof

Varying the background P does not strongly influence the overall shape of the boudins, neither has it an effect on the pressure distribution between boudins and matrix. However, the absolute P values shift with the same amount as the background P is varied. In order to reach the peak P of 1.8 to 1.9 GPa determined based on sample 20GP10, a background P of 1.6 to 1.8 is required.

Other parameters that influence the stress and pressure field include the angle between the long axis of the strong layer and the orientation of the principal stress applied (see Moulas et al., 2014) as well as the aspect ratio of the strong layer (Luisier et al., 2019b). Over-pressure would be generated for a strong layer set at angle $0° < \alpha < 45°$ to the principal stress, whereas under-pressure is generated for the same strong layer if set at angle $45° < \alpha < 90°$ to the principal stress. In our case, the pre-Alpine foliation in the low-strain paragneiss is sub-horizontal and the Alpine foliation in the high-strain paragneiss is sub-vertical. Moreover, the regional foliation southward of the shear zone dips between 70° and 80°. Consequently, the angle α was close to 70° - 90° (Le Bayon and Ballèvre, 2006), which is coherent with the numerical models showing the development of under-pressure in the strong layer. As long as the aspect ratio of the layer is larger than 2, this parameter does not affect the modelled pressure (Luisier et al., 2019a). Furthermore, the rheological contrast, i.e., the viscosity contrast, between the layer and the matrix is also a parameter that influences the magnitude of the pressure variation in the domain (Moulas et al., 2014).

Overall, both the first order shape of the outcrop and metamorphic P distribution determined based on quantitative phase petrology can be reproduced by the model. Therefore, the results of the modelling show that a small difference in H_2O content between two materials of the same composition (here, anorthite dry and wet) results in a significant rheological perturbation, that can locally lead to variations in the tectonic P and strain, under otherwise normal geological background conditions. Moreover, the results confirm that the deformation

and metamorphic evolution of the low Alpine strain paragneiss 20GP07 was constrained by an exceptionally strong rheology and therefore, the results agree with these rocks being H_2O undersaturated.

Consequently, the traditional interpretation that the slow kinetics due to H_2O undersaturated conditions inhibits the formation of high *P* mineral assemblage is here not required anymore, as the exact same argument of H_2O undersaturation can be used to demonstrate that *P* in the unstrained area did potentially never reach the 1.9 GPa as in the shear zone paragneiss, and potentially never even passed the albite breakdown reaction at 1.4 GPa. This relies on the assumption that albite is a secondary product in the deformed paragneiss (where all Na-bearing phases predicted to be stable at H*P* have been lost during decompression), while albite was still stable at peak *P* in the undeformed domain.

The effect of contrasting H_2O saturation conditions on petrology and mechanical behavior of deforming adjacent rocks can be illustrated using a simple sketch (Fig. 10), that displays the main cause to effect relationships. Two simplified rocks are considered, with rock A (Fig. 10A) depicting a H_2O saturated rock, such as the shear zone paragneiss, and rock B (Fig. 10B) a H_2O undersaturated rock, such as the low-strain paragneiss. For the rock A, a schematic phase diagram is drawn, with one dehydration reaction, that separates a field with a hydrous assemblage on the left side from a field with an anhydrous assemblage on the right side. The dehydration reactions is of a type A (hydrous) = B (anhydrous) + H_2O (aq.). For the purpose of the discussion, it is assumed that the fluid produced by the reaction either leaves the system after the reaction has occurred, for example during the deformation, or is present in the rock in a very small volume of pores. In the hydrous field, reactions are kinetically enhanced and symbolized by solid arrows, whereas in the anhydrous field, they are kinetically hindered and symbolized by the dashed arrows.

Journal Pre-proof

The dashed stars represent the L*P*-H*T* conditions reached during the Variscan orogeny. In both cases, it lies in the anhydrous field. During post-Variscan cooling, they reach L*P*-L*T* conditions (empty solid stars), where rock A is hydrated during interaction with externally-derived fluids, whereas rock B remains dry. During the Alpine prograde increase in *P* and *T*, rock A dehydrates along the black arrow going from the blue star to the black star, until it crosses the reaction and reaches the Alpine peak *P*-*T* conditions, labelled P_A. From there, any reaction on the retrograde path during the exhumation would require H_2O addition from an external source in order to allow for equilibration at lower *P*-*T* conditions. In the H_2O saturated rock, the activity of the component H_2O in the fluid phase, a_{H_2O}, is equal to 1. Under high a_{H_2O}, the hydrolytic weakening effect leads to a reduction of the differential stress of the rock (i.e., the difference between the largest and the smallest principal stress), as illustrated on the Mohr circle by the black circle (Fig. 10). For rock B, the same dehydration reaction as in the case A is shown on the schematic phase diagram for a H_2O undersaturated rock (the reaction separating the blue and grey field), however it is shifted towards lower *T*, as we now have $a_{H_2O} < 1$ (Thompson, 1983). Hence, the stability field of the dry assemblage is larger. At conditions of $a_{H_2O} < 1$, the hydrolytic weakening effect is reduced or absent and rock B is mechanically stronger than rock A. Therefore, the differential stress of rock B is larger than of rock A. In order to satisfy the force balance, as rocks A and B are in contact, under compression, both circles touch on the side of the maximal principal stress, such that the mean stress in rock B, corresponding to the *P* of rock B, P_B, is lower than that of rock A, P_A. From this graphical illustration, we see that units that have adjacent, mechanically heterogeneous, rocks experience different stress states, leading to different *P*. In turn, this strength contrast controls the strain localization, with weaker domains preferentially affected by deformation. Therefore, this schematic sketch can be used to explain both the petrological

data and structural observations from the Gran Paradiso adjacent H_2O (under)-saturated paragneisses.

The previous studies that have explained outcrop scale metamorphic *P* variations with stress-induced *P* perturbations were based on similar assumptions that the coexisting rocks have strength contrasts sufficiently large to generate measurable metamorphic *P* variations. For example, the strength contrast in the study of Jamtveit et al. (2018) corresponds to a viscosity ratio of 10 between the host granulite and the eclogitic shear zone. Luisier et al. (2019) use a viscosity ratio of 100 between the strong metagranite and the weak whiteschists. Here, the strength contrast between the strong layer and the matrix corresponds to an effective viscosity ratio of 10 at the beginning of the simulation and it increases up to a ratio of 1000 during the formation of the boudins (Supplementary Material S2). Consequently, simulating deformation of materials of variable viscosities, such as weak whiteschist or eclogite versus strong granite or granulite, leads to *P* deviations of the same order of magnitude as for deformation of materials of fixed composition but with different H_2O content.

Finally, the methodology used in this study could be applied to other potentially H_2O deficient parts of the nappe, such as the metagranites, that were locally also not strongly deformed and in which the assemblage jadeite + quartz has never been reported.

Conclusion

This study emphasizes the importance of considering mechanical stresses when non-equilibrium processes are suspected in metamorphic rocks. Quantitative phase petrology allowed to recognize the key role of H_2O in explaining the variation in peak metamorphic conditions between the shear zone paragneiss and the low Alpine strain paragneiss from the Gran Paradiso Unit. Under closed system conditions, the initial H_2O content of the protolith as well as the slope of the H_2O isopleths in the *P*–*T* space determine the ability of the rock to

react on the prograde path and equilibrate to H*P* conditions in continental collision settings. This combined thermodynamic and numerical modelling study confirms that besides its role on reaction kinetics, H_2O has a strong impact on the mechanical behavior of rocks under stress. Our large-scale model results corroborate the previously experimentally determined behavior of dry versus wet rocks subjected to deformation. Our models highlight the fact that local differences in H_2O saturation conditions in rocks of an otherwise same composition lead to significant strain and *P* variations over geological timescales, such that metamorphic rocks can record this difference in peak conditions. We show that kinetics is not necessarily the limiting factor to the development of H*P* mineral parageneses and that H*P* conditions may not even be generated in portions of nappes that evolve under H_2O undersaturated conditions. Past metamorphic events and more generally the tectono-metamorphic heritage has a strong impact on the H_2O budget of rocks, hence these portions of tectonic nappes have an inherited history that influences their metamorphic and mechanical evolution during further metamorphic events. The knowledge of the past metamorphic history of H*P* units is thus important when considering local variations in strain and metamorphic conditions.

Acknowledgements

C. Luisier thanks Paola Manzotti for assistance during field work, Pavel Pitra for the interesting discussions and advice regarding the thermodynamic modelling part, Philippe Yamato for discussions on the thermo-mechanical modelling, Xavier Le Coz for sample preparation, and Martin Robyr and Jessica Langlade for assistance during EPMA acquisition. We thank Simon Schorn, Pierre Lanari and one anonymous reviewer for their detailed and constructive reviews, as well as Nadia Malaspina for the editorial handling of the manuscript.

Competing interest declaration

Journal Pre-proof

The authors declare no competing interests.

References

Ahrens, T.J., Schubert, G., 1975. Gabbro-eclogite reaction rate and its geophysical significance. Reviews of Geophysics and Space Physics 13, 383–400.

Austrheim, H., 1987. Eclogitization of lower crustal granulites by fluid migration through shear zones. Earth and Planetary Science Letters 81, 221–232.

Austrheim, H., Griffin, W.L., 1985. Shear deformation and eclogite formation within granulite-facies anorthosites of the Bergen Arcs, western Norway. Chemical Geology 50, 267–281.

Auzanneau, E., Schmidt, M.W., Vielzeuf, D., Connolly, J. a. D., 2010. Titanium in phengite: a geobarometer for high temperature eclogites. Contrib Mineral Petrol 159, 1.

Baldwin, J.A., Powell, R., Brown, M., Moraes, R., Fuck, R.A., 2005. Modelling of mineral equilibria in ultrahigh-temperature metamorphic rocks from the Anápolis–Itauçu Complex, central Brazil. Journal of Metamorphic Geology 23, 511–531.

Ballèvre, M., 1986. Collision continentale et chemins P-T. L'unité pennique du Grand Paradis (Alpes occidentales). Université de Rennes 1, Rennes.

Bertrand, J.M., Paquette, J.-L., Guillot, F., 2006. Permian zircon U-Pb ages in the Gran Paradiso massif: revisiting post-Variscan events in the Western Alps.

Biino, G., Pognante, U., 1989. Palaeozoic continental-type gabbros in the Gran Paradiso nappe (Western Alps, Italy): Early-Alpine eclogitization and geochemistry. Lithos 24, 3–19.

Borghi, A., Compagnoni, R., Sandrone, R., 1996. Composite P-T paths in the internal Penninic massifs of the western Alps: Petrological constraints to their thermo-mechanical evolution. Eclogae Geol. Helv. 89, 345–367.

Brouwer, F., Vissers, R., Lamb, W., 2002. Structure and metamorphism of the Gran Paradiso massif, western Alps, Italy. Contrib Mineral Petrol 143, 450–470.

Carlson, W.D., 2010. Dependence of reaction kinetics on H2O activity as inferred from rates of intergranular diffusion of aluminium. Journal of Metamorphic Geology 28, 735–752.

Chu, X., Ague, J.J., Podladchikov, Y.Y., Tian, M., 2017. Ultrafast eclogite formation via melting-induced overpressure. Earth and Planetary Science Letters 479, 1–17.

Cionoiu, S., Moulas, E., Tajčmanová, L., 2019. Impact of interseismic deformation on phase transformations and rock properties in subduction zones. Sci Rep 9, 1–6.

Compagnoni, R., Elter, G., Lombardo, B., 1974. Eterogeneita stratigrafica del complesso degli "gneiss minuti" nel massiccio cristallino del Gran Paradiso. Memorie della Società

Journal Pre-proof

Geologica Italiana 13, 227–239.

Compagnoni, R., Lombardo, B., 1974. The Alpine age of the Gran Paradiso eclogites. Rendiconti Societá Italiana Di Mineralogia E Petrologia 30, 220–237.

Compagnoni, R., Prato, R., 1969. Paramorfosi di cianite su sillimanite in scisti pregranitici del massicio del Gran Paradiso. Bol. Soc. Geol. It. 88, 537–549.

Connolly, J.A.D., Podladchikov, Y.Y., 2013. A Hydromechanical Model for Lower Crustal Fluid Flow, in: Harlov, D.E., Austrheim, H. (Eds.), Metasomatism and the Chemical Transformation of Rock: The Role of Fluids in Terrestrial and Extraterrestrial Processes, Lecture Notes in Earth System Sciences. Springer, Berlin, Heidelberg, pp. 599–658.

Dal Piaz, G.V., Lombardo, B., 1986. Early Alpine eclogite metamorphism in the Penninic Monte Rosa-Gran Paradiso basement nappes of the northwestern Alps. Geological Society of America Memoirs 164, 249–266.

de Capitani, C., Brown, T.H., 1987. The computation of chemical equilibrium in complex systems containing non-ideal solutions. Geochimica et Cosmochimica Acta 51, 2639–2652.

Deer, W.A., Howie, R.A., Zussman, J., 2013. An Introduction to the Rock Forming Minerals., 3rd Edition. ed. Mineralogical Society of Great Britain & Ireland, UK.

Duretz, T., de Borst, R., Yamato, P., 2021. Modeling Lithospheric Deformation Using a Compressible Visco-Elasto-Viscoplastic Rheology and the Effective Viscosity Approach. Geochemistry, Geophysics, Geosystems 22, e2021GC009675.

Ferry, J.M., Burt, D.M., 1982. Characterization of metamorphic fluid composition through mineral equilibria. Reviews in Mineralogy and Geochemistry 10, 207–262.

Fyfe, W.S., Price, N.J., Thompson, A.B., 1978. Fluids in the Earth's crust. Their significance in metamorphic, tectonic and chemical transport mechanisms. Elsevier (Developments in Geochemistry, 1), Amsterdam.

Gabudianu Radulescu, I., Compagnoni, R., Lombardo, B., 2011. Polymetamorphic history of a relict Permian hornfels from the central Gran Paradiso Massif (Western Alps, Italy): a microstructural and thermodynamic modelling study: Polymetamorphic History of Relict Permian Hornfels. Journal of Metamorphic Geology 29, 851–874.

Gasco, I., Borghi, A., Gattiglio, M., 2010. Metamorphic evolution of the Gran Paradiso Massif: A case study of an eclogitic metagabbro and a polymetamorphic glaucophane–garnet micaschist. Lithos 115, 101–120.

Green, E.C.R., White, R.W., Diener, J.F.A., Powell, R., Holland, T.J.B., Palin, R.M., 2016. Activity–composition relations for the calculation of partial melting equilibria in metabasic rocks. Journal of Metamorphic Geology 34, 845–869.

Griggs, D., 1967. Hydrolytic Weakening of Quartz and Other Silicates*. Geophysical Journal International 14, 19–31.

Journal Pre-proof

Holland, T.J.B., 1980. The reaction albite = jadeite+quartz determined experimentally in the range 600-1200 degrees C. American Mineralogist 65, 129–134.

Holland, T.J.B., Powell, R., 2011. An improved and extended internally consistent thermodynamic dataset for phases of petrological interest, involving a new equation of state for solids. Journal of Metamorphic Geology 29, 333–383.

Jamtveit, B., Moulas, E., Andersen, T.B., Austrheim, H., Corfu, F., Petley-Ragan, A., Schmalholz, S.M., 2018. High Pressure Metamorphism Caused by Fluid Induced Weakening of Deep Continental Crust. Scientific Reports 8, 17011.

Joachim, B., Heinrich, W., Höschen, C., Abart, R., 2019. The effect of H2O fluid on relative component mobilities in a bimineralic reaction rim in the system CaO–MgO–SiO2. European Journal of Mineralogy 31, 61–72.

Kiss, D., Podladchikov, Y., Duretz, T., Schmalholz, S.M., 2019. Spontaneous generation of ductile shear zones by thermal softening: Localization criterion, 1D to 3D modelling and application to the lithosphere. Earth and Planetary Science Letters 519, 284–296.

Koch, P.S., Christie, J.M., Ord, A., George Jr., R.P., 1989. Effect of water on the rheology of experimentally deformed quartzite. Journal of Geophysical Research: Solid Earth 94, 13975–13996.

Lanari, P., Ferrero, S., Goncalves, P., Groppo, C., 2019. Metamorphic geology: progress and perspectives. Geological Society, London, Special Publications 478, 1–12.

Le Bayon, B., 2005. Evolution structurale et métamorphique d'une croûte continentale subductée (Grand Paradis, Alpes occidentales). PhD Thesis, University of Rennes 1, Rennes.

Le Bayon, B., Ballèvre, M., 2006. Deformation history of a subducted continental crust (Gran Paradiso, Western Alps): continuing crustal shortening during exhumation. Journal of Structural Geology 28, 793–815.

Le Bayon, B., Pitra, P., Ballèvre, M., Bohn, M., 2006. Reconstructing P–T paths during continental collision using multi-stage garnet (Gran Paradiso nappe, Western Alps). Journal of Metamorphic Geology 24, 477–496.

Luisier, C., 2018. Pressure variations in the Monte Rosa nappe, Western Alps. PhD Thesis, Lausanne University, Lausanne.

Luisier, C., Baumgartner, L., Schmalholz, S.M., Siron, G., Vennemann, T., 2019a. Metamorphic pressure variation in a coherent Alpine nappe challenges lithostatic pressure paradigm. Nat Commun 10, 1–11.

Luisier, C., Baumgartner, L., Schmalholz, S.M., Siron, G., Vennemann, T., 2019b. Metamorphic pressure variation in a coherent Alpine nappe challenges lithostatic pressure paradigm. Nat Commun 10, 1–11.

Mancktelow, N.S., 2008. Tectonic pressure: Theoretical concepts and modelled examples. Lithos, Rocks Generated under Extreme Pressure and Temperature Conditions: Mechanisms,

Journal Pre-proof

Concepts, Models 103, 149–177.

Mancktelow, N.S., 1995. Nonlithostatic pressure during sediment subduction and the development and exhumation of high pressure metamorphic rocks. Journal of Geophysical Research: Solid Earth 100, 571–583.

Manzotti, P., Bosse, V., Pitra, P., Robyr, M., Schiavi, F., Ballèvre, M., 2018. Exhumation rates in the Gran Paradiso Massif (Western Alps) constrained by in situ U–Th–Pb dating of accessory phases (monazite, allanite and xenotime). Contrib Mineral Petrol 173, 24.

Manzotti, P., Pitra, P., Langlade, J., Ballèvre, M., 2015. Constraining P–T conditions during thrusting of a higher pressure unit over a lower pressure one (Gran Paradiso, Western Alps). Journal of Metamorphic Geology 33, 981–1002.

Manzotti, P., Veslud, C.L.C.D., Bayon, B.L., Ballèvre, M., 2014. Petro-structural map of the Money Unit (Gran Paradiso Massif, Valnontey valley, Western Alps). Journal of Maps 10, 324–340.

Massonne, H.-J., 2015. Derivation of P–T paths from high pressure metagranites — Examples from the Gran Paradiso Massif, western Alps. Lithos.

Massonne, H.-J., Schreyer, W., 1987. Phengite geobarometry based on the limiting assemblage with K-feldspar, phlogopite, and quartz. Contr. Mineral. and Petrol. 96, 212–224.

Michard, A., Schmid, S.M., Lahfid, A., Ballèvre, M., Manzotti, P., Chopin, C., Iaccarino, S., Dana, D., 2022. The Maira-Sampeyre and Val Grana Allochthons (south Western Alps): review and new data on the tectonometamorphic evolution of the Briançonnais distal margin. Swiss Journal of Geosciences 115, 19.

Milke, R., Neusser, G., Kolzer, K., Wunder, B., 2013. Very little water is necessary to make a dry solid silicate system wet. Geology 41, 247–250.

Moulas, E., Burg, J.-P., Podladchikov, Y., 2014. Stress field associated with elliptical inclusions in a deforming matrix: Mathematical model and implications for tectonic overpressure in the lithosphere. Tectonophysics, Observational and Modelling perspectives on the Mechanical properties of the Lithosphere 631, 37–49.

Moulas, E., Podladchikov, Y.Y., Aranovich, L.Y., Kostopoulos, D., 2013. The problem of depth in geology: When pressure does not translate into depth. Petrology 21, 527–538.

Nosenzo, F., Manzotti, P., Poujol, M., Ballèvre, M., Langlade, J., 2022. A window into an older orogenic cycle: P–T conditions and timing of the pre-Alpine history of the Dora-Maira Massif (Western Alps). Journal of Metamorphic Geology 40, 4, 789-821.

Passchier, C.W., Trouw, R.A.J. (Eds.), 2005. Foliations, Lineations and Lattice Preferred Orientation, in: Microtectonics. Springer, Berlin, Heidelberg, pp. 67–109.

Pattison, D.R.M., De Capitani, C., Gaidies, F., 2011. Petrological consequences of variations in metamorphic reaction affinity. Journal of Metamorphic Geology 29, 953–977.

Journal Pre-proof

Proyer, A., 2003. The preservation of high-pressure rocks during exhumation: metagranites and metapelites. Lithos, 6th International Eclogite Conference: Eclogites and Related High and Ultrahigh Pressure Metamorphic Rocks 70, 183–194.

Putnis, A., 2021. Fluid-mineral interactions: Controlling coupled mechanisms of reaction, mass transfer and deformation. Journal of Petrology.

Remmert, P., Heinrich, W., Wunder, B., Morales, L., Wirth, R., Rhede, D., Abart, R., 2017. Synthesis of monticellite–forsterite and merwinite–forsterite symplectites in the CaO–MgO–SiO2 model system: influence of temperature and water content on microstructure evolution. Contrib Mineral Petrol 173, 5.

Rieder, M., Cavazzini, G., D'yakonov, Y.S., Frank-Kamenetskii, V.A., Gottardi, G., Guggenheim, S., Koval, P.V., Mueller, G., Neiva, A.M.R., Radoslovich, E.W., Robert, J.L., Sassi, F.P., Takeda, H., Weiss, Z., Wones, D.R., 1999. Nomenclature of the micas. Mineralogical Magazine 63, 267–279.

Ring, U., Collins, A.S., Kassem, O.K., 2005. U-Pb SHRIMP data on the crystallization age of the Gran Paradiso augengneiss, Italian Western Alps: Further evidence for Permian magmatic activity in the Alps during break-up of Pangea. Eclogae geol. Helv. 98, 363–370.

Rubie, D.C., 1998. Disequilibrium during metamorphism: the role of nucleation kinetics, in: Taylor, P.J., Obrien, P.J. (Eds.), What Drives Metamorphism and Metamorphic Reactions? Geological Soc Publishing House, Bath, pp. 193–214.

Rubie, D.C., 1986. The catalysis of mineral reactions by water and restrictions on the presence of aqueous fluid during metamorphism. Mineralogical Magazine 50, 399–415.

Rybacki, E., Dresen, G., 2004. Deformation mechanism maps for feldspar rocks. Tectonophysics 382, 173–187.

Rybacki, E., Dresen, G., 2000. Dislocation and diffusion creep of synthetic anorthite aggregates. Journal of Geophysical Research: Solid Earth 105, 26017–26036.

Rybacki, E., Gottschalk, M., Wirth, R., Dresen, G., 2006. Influence of water fugacity and activation volume on the flow properties of fine-grained anorthite aggregates. J. Geophys. Res. 111, B03203.

Schenker, F.L., Schmalholz, S.M., Moulas, E., Pleuger, J., Baumgartner, L.P., Podladchikov, Y., Vrijmoed, J., Buchs, N., Müntener, O., 2015. Current challenges for explaining (ultra)high-pressure tectonism in the Pennine domain of the Central and Western Alps. J. Metamorph. Geol. 33, 869–886.

Schmalholz, S.M., Podladchikov, Y., 2014. Metamorphism under stress: The problem of relating minerals to depth. Geology 42, 733–734.

Schmidt, M.W., Poli, S., 1998. Experimentally based water budgets for dehydrating slabs and consequences for arc magma generation. Earth and Planetary Science Letters 163, 361–379.

Schorn, S., 2022. Self-induced incipient 'eclogitization' of metagranitoids at closed-system

Journal Pre-proof

conditions. Journal of Metamorphic Geology.

Schorn, S., 2018. Dehydration of metapelites during high-P metamorphism: The coupling between fluid sources and fluid sinks. Journal of Metamorphic Geology 36, 369–391.

Tajčmanová, L., Podladchikov, Y., Powell, R., Moulas, E., Vrijmoed, J. c., Connolly, J. a. d., 2014. Grain-scale pressure variations and chemical equilibrium in high-grade metamorphic rocks. J. Meta. Geol. 32, 195–207.

Tajčmanová, L., Vrijmoed, J., Moulas, E., 2015. Grain-scale Pressure Variations in Metamorphic Rocks: Implications for the Interpretation of Petrographic Observations. Lithos 216–217, 338–351.

Thompson, A.B., 1983. Fluid-absent metamorphism. Journal of the Geological Society 140, 533–547.

Vaughan-Hammon, J.D., Luisier, C., Baumgartner, L.P., Schmalholz, S.M., 2021. Peak Alpine metamorphic conditions from staurolite-bearing metapelites in the Monte Rosa nappe (Central European Alps) and geodynamic implications. Journal of Metamorphic Geology 39, 897–917.

Vrijmoed, J.C., Podladchikov, Y.Y., Andersen, T.B., Hartz, E.H., 2009. An alternative model for ultra-high pressure in the Svartberget Fe-Ti garnet-peridotite, Western Gneiss Region, Norway. European Journal of Mineralogy 21, 1119–1133.

Warr, L.N., 2021. IMA–CNMNC approved mineral symbols. Mineralogical Magazine 85, 291–320.

Wayte, G.J., Worden, R.H., Rubie, D.C., Droop, G.T.R., 1989. A TEM study of disequilibrium plagioclase breakdown at high pressure: the role of infiltrating fluid. Contributions to Mineralogy and Petrology 101, 426–437.

White, R.W., Powell, R., Holland, T.J.B., Johnson, T.E., Green, E.C.R., 2014. New mineral activity–composition relations for thermodynamic calculations in metapelitic systems. Journal of Metamorphic Geology 32, 261–286.

Wong, L.N.Y., Maruvanchery, V., Liu, G., 2016. Water effects on rock strength and stiffness degradation. Acta Geotech. 11, 713–737.

Tables and Figures

Table 1 Representative mineral compositions and modes for major phases in 20GP10 and calculated local bulk rock composition

	Garnet V	Garnet A mantle	Garnet A rim	Plagioclase	Phengite	Phengite max Si	Biotite	Chlorite	Bulk rock*
SiO_2	37.04	38.08	37.15	60.80	50.42	53.59	37.48	25.60	60.28
TiO_2	0.16	0.16	0.03		0.32	0.24	1.93	0.07	1.18

Al_2O_3	20.53	21.08	21.08	24.54	27.88	25.44	16.96	20.58	17.78
FeO	20.91	27.65	30.29	0.09	0.72	1.16	0.00	28.20	5.67
Fe_2O_3	0.16	0.29	1.10		1.77	1.56	19.54		1.80
MnO	11.51	0.99	2.01						0.19
MgO	1.04	1.89	2.76		3.06	3.65	10.42	12.83	2.65
CaO	7.67	10.55	5.55	6.18	0.00	0.05	0.04	0.01	2.40
Na_2O	0.04	0.03	0.02	7.95	0.40	0.20	0.05	0.00	0.99
K_2O				0.10	10.85	10.29	10.12	0.03	4.53
H_2O**					4.58	3.79	3.46	12.68	2.53
Total	**99.06**	**100.72**	**99.99**	**99.66**	**100.00**	**100.00**	**100.00**	**100.00**	**100.00**
Mode	2	8	5	10	35		5	5	
	* Local Bulk rock calculated with additional 25% quartz, 2% titanite and 0.3% rutile and by substracting the garnet cores								
** H2O calculated as the difference between 100 and the sum of oxydes									

Table 2 Representative mineral compositions and modes for major phases in 20GP07 and calculated local bulk rock composition

	Phengite	Phengite max Si	Muscovite	Garnet	Plagioclase	Biotite	Chlorite	Bulk rock*
SiO2	50.39	52.22	46.52	36.29	68.21	49.73	26.49	50.29
TiO2	0.18	0.17	0.37	0.86		0.48	0.01	0.33
Al2O3	27.38	25.20	32.82	20.33	19.91	27.58	21.17	26.94
FeO	3.41	3.70	3.26	32.37	0.16	5.96	19.48	6.98
Fe2O3								0.00
MnO	0.00	0.00	0.00	1.10		0.02	0.23	0.15
MgO	3.17	3.67	1.20	3.32		3.96	19.88	2.02
CaO	0.01	0.01	0.00	6.43	0.27	0.19	0.03	0.92
Na2O	0.38	0.33	0.94	0.01	11.44	0.33	0.00	2.51
K2O	10.48	9.86	10.17	0.00	0.02	9.33	0.01	6.62
H2O**	4.60	4.71	4.74			2.42	12.71	3.24
Total	**100.00**	**100.00**	**100.00**	**100.77**	**100.01**	**100.00**	**100.00**	**100.00**
Mode	15		20	10	17	3	5	
	* Local bulk rock calculated with additional 30% quartz							
	** H2O calculated as the difference between 100 and the sum of oxydes							

Table 3 Parameters used in the reference 2D thermo-mechanical model

Parameter	**Symbol**	**Units**	**Whole model**	
Temperature	T	K	793.15	
Cohesion	C	Pa	2e7	
Friction angle	φ	°	30	
Shear modulus	G	Pa	1e10	
Thermal conductivity	k	$W \cdot m^{-1} \cdot K^{-1}$	2.3	
Heat capacity	C_p	$J \cdot kg^{-1} \cdot K^{-1}$	1050	
Dislocation creep*			**Matrix (An100, 0.07 %**	**Layer (An100, 0.004 %**

Journal Pre-proof

			H_2O)	H_2O)
Pre-exponential factor	A	$Pa^{-n}\cdot s^{-1}$	3.9811×10^{-16}	5.0119×10^{-6}
Exponent	n	-	3	3
Activation Energy	Q	$J\cdot mol^{-1}$	356×10^{3}	648×10^{3}
Density	ρ	$kg\cdot m^{-3}$	3300	2800

* Parameters for matrix and layer are those of anorthite wet and anorthite dry, respectively, from Rybacki and Dresen (2004).

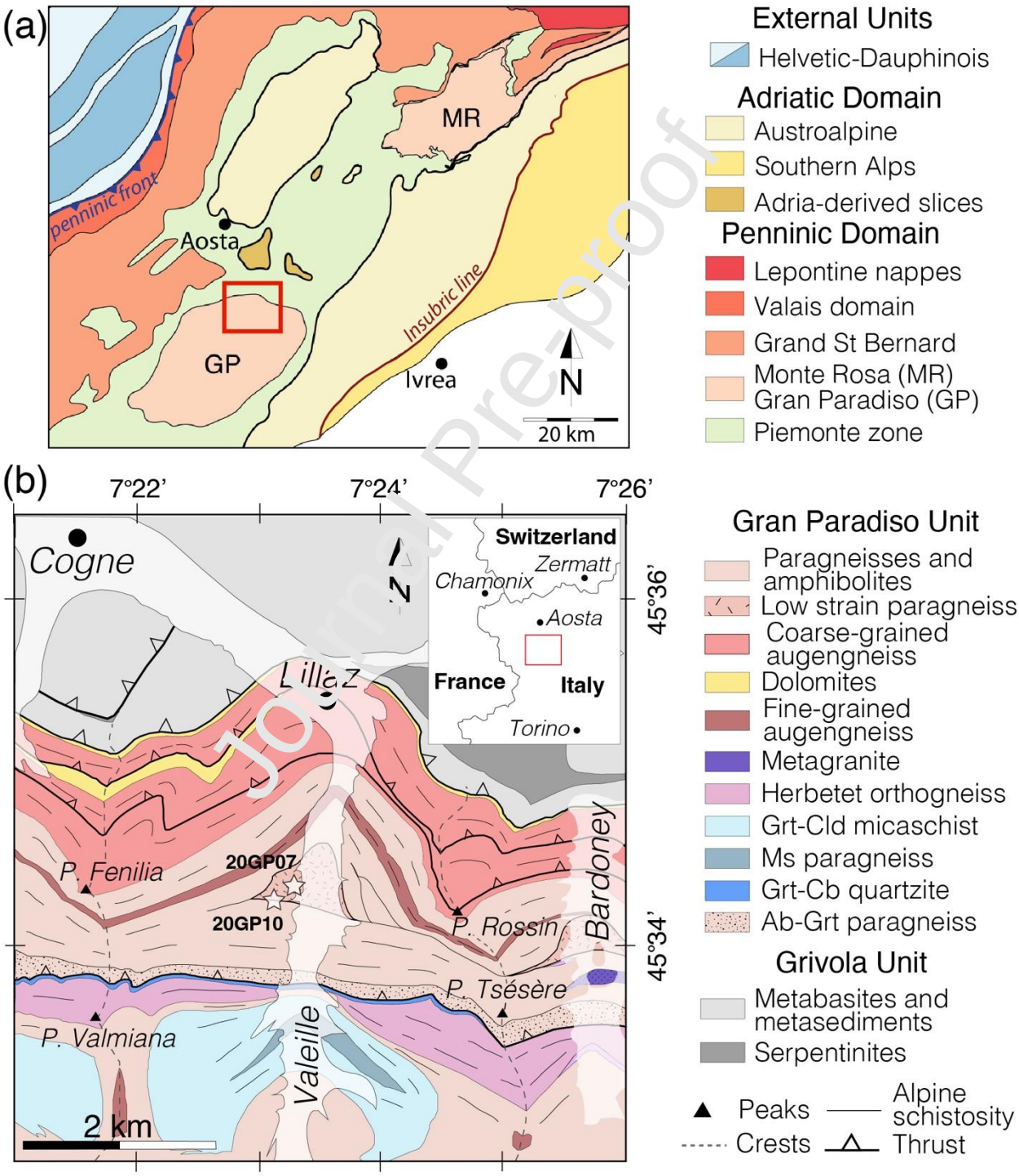

Journal Pre-proof

Figure 1 (a) Simplified tectonic map of the Western Alps (modified after Steck et al., 2015). The study area is located in the North of the Gran Paradiso nappe (GP) and outlined on the map by a square. (b) Simplified geological map of the study area, modified after Le Bayon (2005). The location of the two samples studied (20GP07 and 20GP10) are indicated by stars. 20GP07 was sampled in the low strain paragneiss and 20GP10 in the paragneiss with Alpine schistosity.

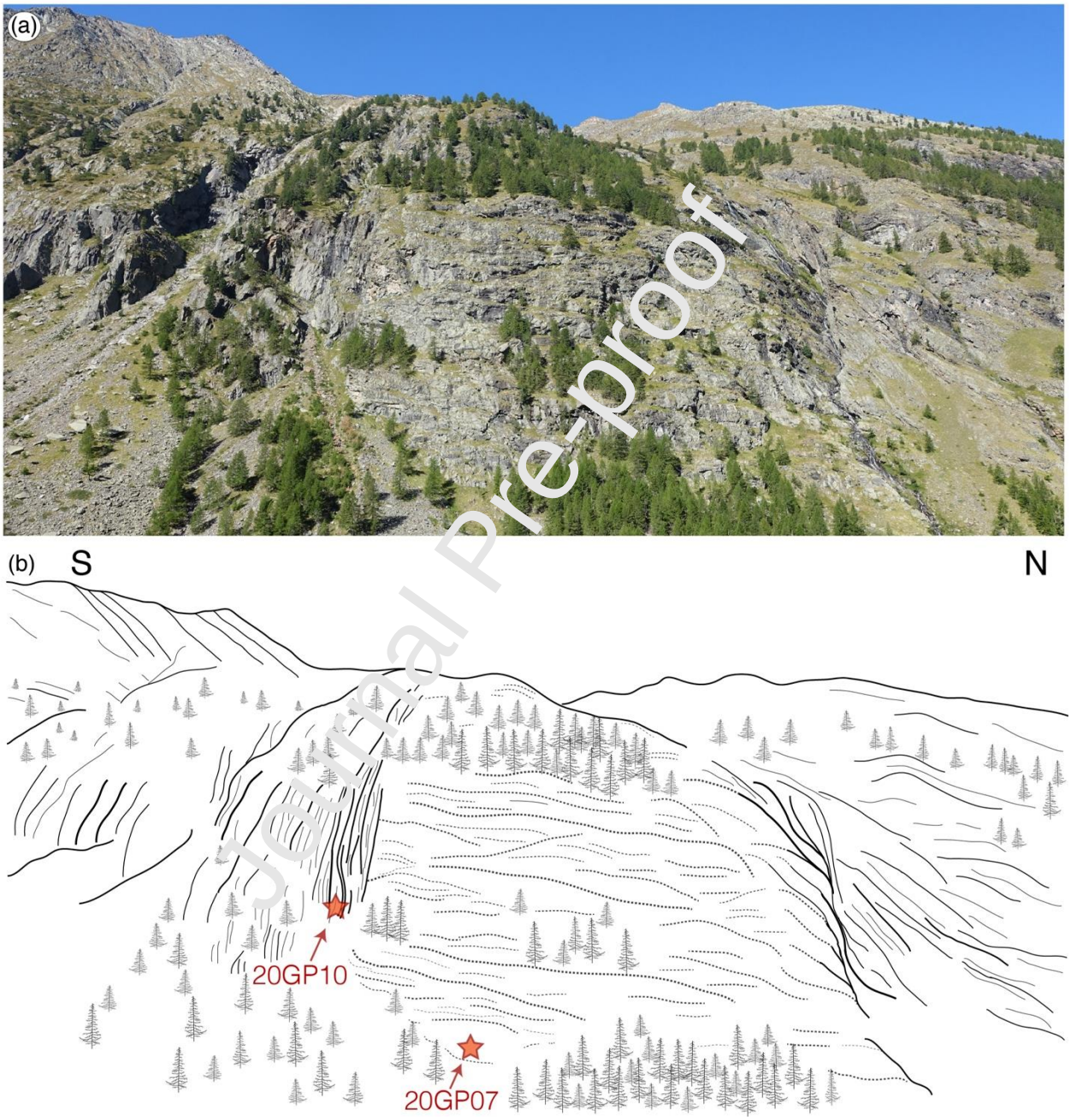

Figure 2 (a) Field picture of the studied outcrops, on the left bank of the Valeille valley in the northern Gran Paradiso massif. (b) Corresponding sketch of the main structural characteristics deduced from the field observations. The straight lines represent the Alpine schistosity in the paragneiss, whereas the dashed lines show the pre-Alpine foliation and represent the Alpine low-strain paragneiss represented in the geological map of Fig. 1b. The sample 20GP07 was taken in the pre-Alpine paragneiss and sample 20GP10 was taken in the Alpine shear zone.

Journal Pre-proof

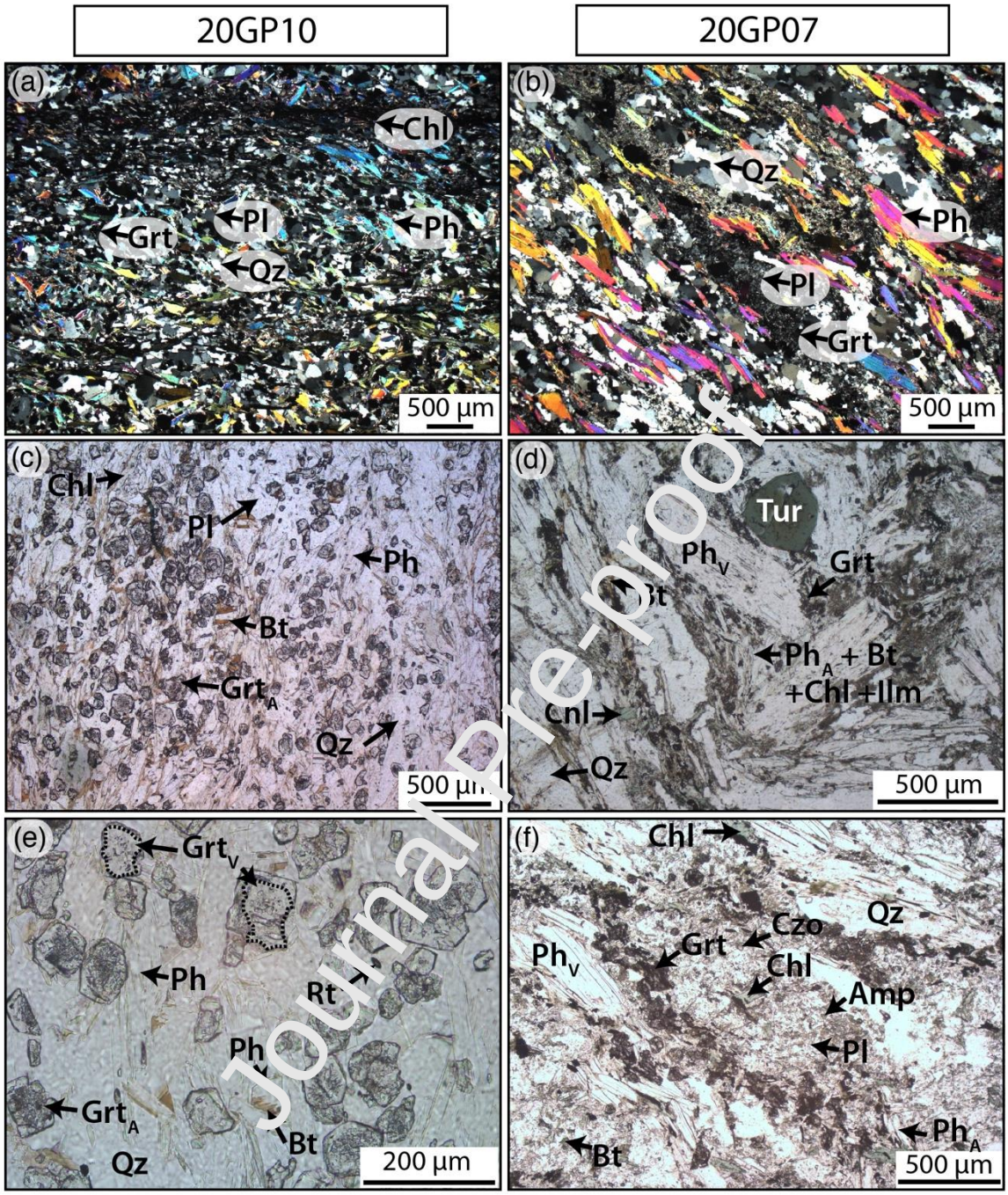

Figure 3 Optical microphotographs showing the representative textures of the shear zone sample 20GP10 (a-c-e) and the low strain paragneiss 20GP07 (b-d-f). (a) Paragneiss 20GP10 has an Alpine schistosity marked by phengite and quartz, wrapping around small Alpine garnets. (b) Paragneiss 20GP07 shows a pre-Alpine schistosity, marked by quartz, large pre-Alpine phengites, and plagioclase pseudomorphs. (c) Late biotite and plagioclase overgrowth the main schistosity. (d) Large pre-Alpine phengite crystals (Ph_V), are surrounded by an Alpine generation of fine-grained intergrowths of phengite (Ph_A), garnet, biotite, chlorite and ilmenite. (e) Detailed view showing inclusion-rich garnet cores surrounded by inclusion-poor rims. Few inclusion-rich Alpine garnets (Grt_A) surround inclusion-free cores, corresponding to a pre-Alpine garnet generation (labelled Grt_v). Rutile is found as inclusion in Alpine garnet as well as in the matrix. Minor, late biotite grows mainly on the tips of phengite. (f) Plagioclase pseudomorphs in 20GP07 consist of fine-grained intergrowths of albite,

clinozoisite, phengite, garnet, amphibole, ± biotite, ± chlorite. Garnet is essentially developed along the outer margin of the pseudomorph.

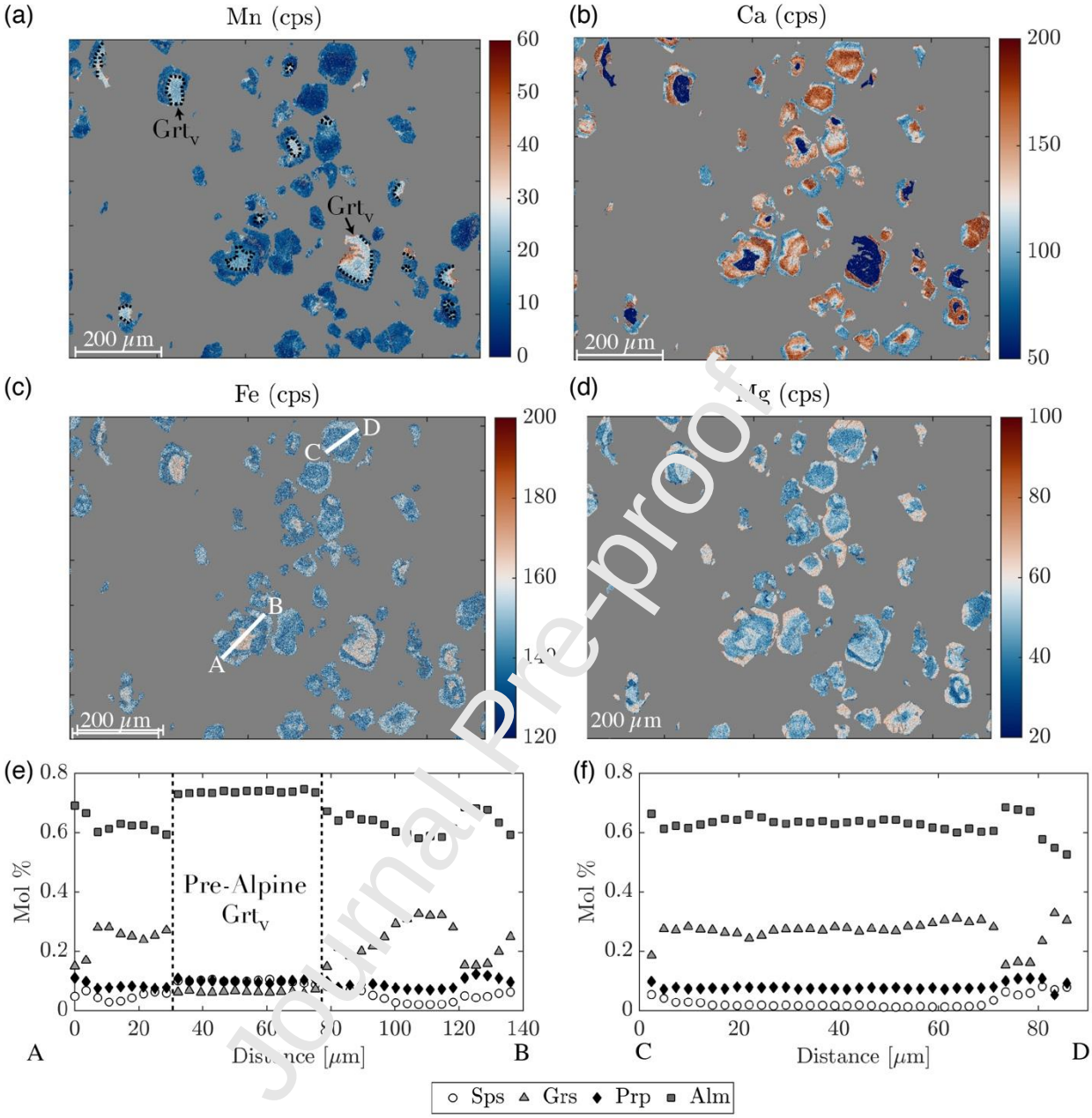

Journal Pre-proof

Figure 4 X-ray maps of garnets in sample 20GP10. (a) Mn (cps). High-Mn garnet cores are resorbed and correspond to pre-Alpine garnets (Grt_V), which served as nuclei for low-Mn Alpine garnets. (b) Similar straight boundary in X-ray intensity between Grt_V cores and Alpine garnet overgrowths can be seen on the Ca signal. Alpine garnets show a high-Ca mantle and a decreasing Ca towards the rims. (c) Fe map also shows an increase in signal from mantle to rim in Alpine garnets. (d) Mg map shows an increase in Mg from mantle to rim in Alpine garnet. Two garnets were selected for profile measurements, one in a garnet enclosing a pre-Alpine core (profile A-B) and one in an Alpine garnet without pre-Alpine core (profile C-D). Profile locations are shown with white traces in (c). (e) and (f) Mole % of the four components along profiles A-B and C-D, respectively.

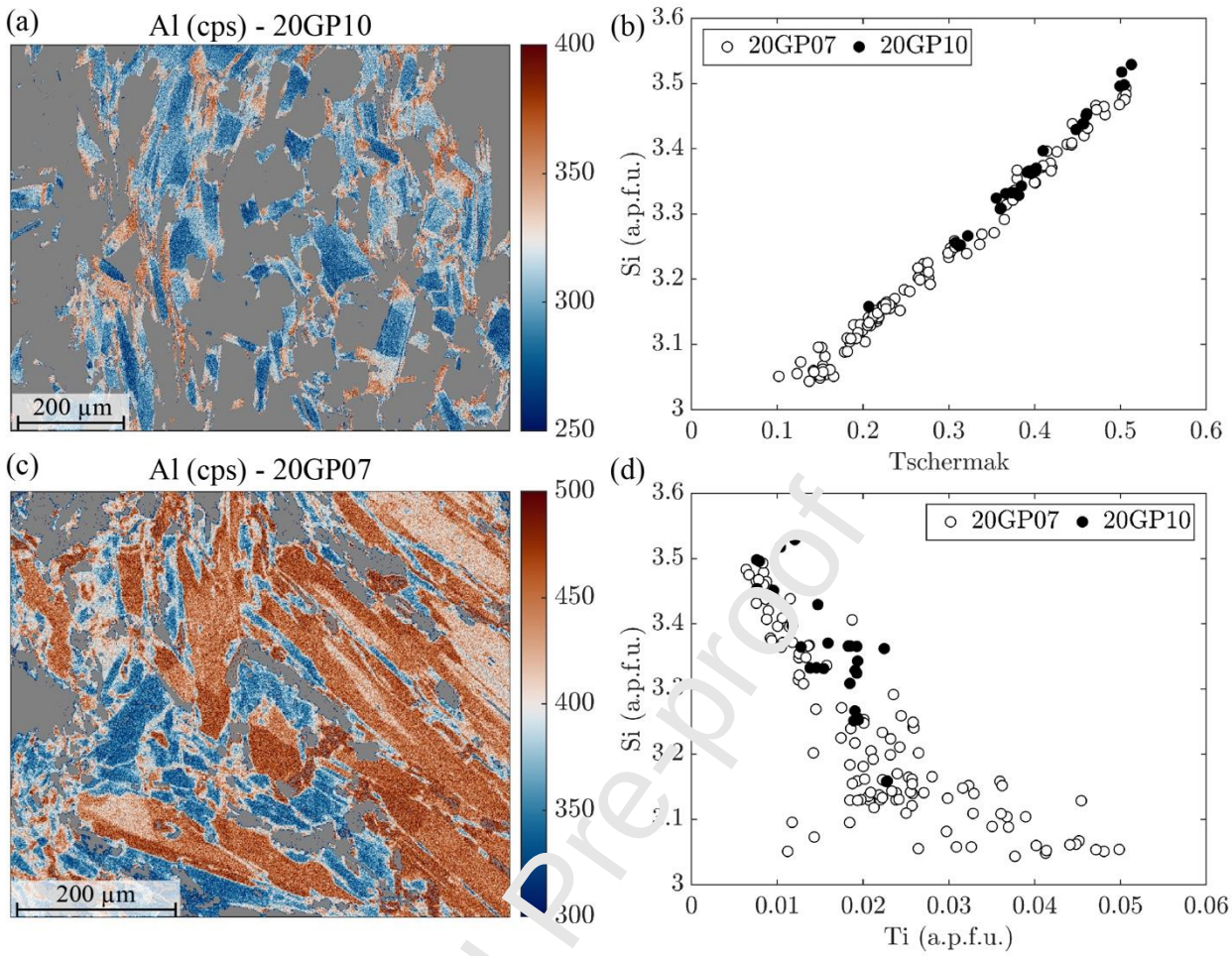

Figure 5 (a) X-ray map of white micas in the same area of 20GP10 as for the garnet X-ray maps in Fig. 4, showing here the Al intensity (cps). White mica cores have low Al contents, whereas rims are richer in Al. (b) Silica (a.p.f.u.) versus Tschermak component in white micas from sample 20GP10 and 20GP07. The correlation indicates a phengitic compositional trend, controlled by the Tschermak exchange. (c) X-ray map of white micas in sample 20GP07, showing the Al intensity (cps). Large white micas (in red) have high Al contents, whereas smaller white micas (in blue) crystallizing between the larger flakes are poorer in Al. (b) Silica (a.p.f.u.) versus titanium content (a.p.f.u.) in white micas from sample 20GP10 and 20GP07. As a whole, the mica composition has a much larger spread in sample 20GP07 than in sample 20GP10, reflecting (i) a much better equilibration in the deformed sample (20GP07), and (ii) the 'metastable' persistence of relict, pre-Alpine, composition in the large flakes from sample 20GP10.

Journal Pre-proof

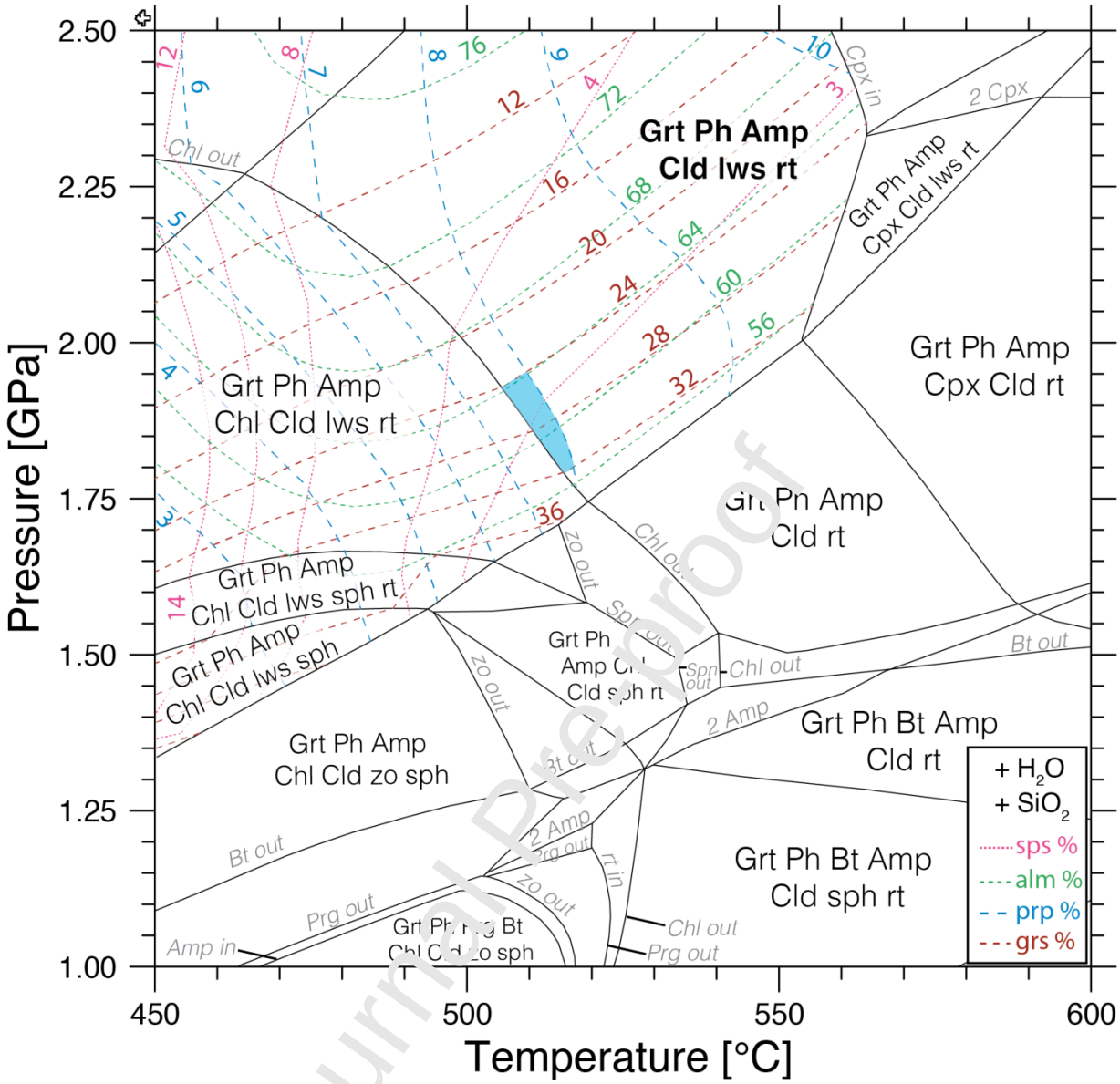

Figure 6 *P-T* pseudosection calculated for a local bulk composition in the shear zone paragneiss 20GP10, using H_2O saturated conditions. Red and blue dashed lines show the grossular (grs), pyrope (prp), spessartine (sps) and almandine (alm) content (in mol%), respectively. The blue field indicates the peak P-T conditions at 500 – 520 °C and 1.80 – 1.95 GPa, based on the garnet chemical composition. Mineral assemblages are written by order of decreasing abundance, with capital letters for phases with variable composition, and lower-case letters for phases considered as pure end-members in the calculation.

Journal Pre-proof

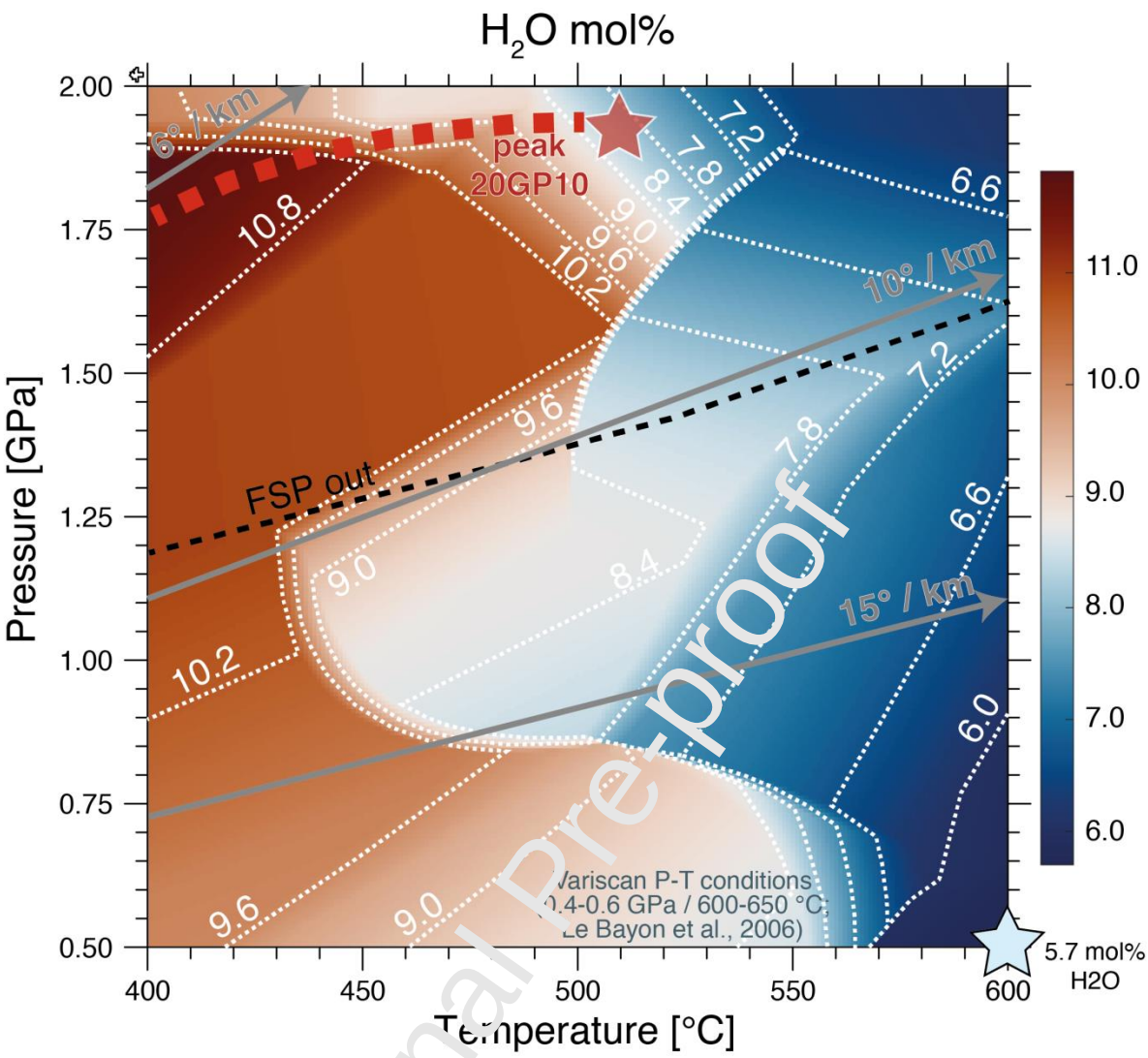

Figure 7 *P-T* pseudosection calculated for sample 20GP07 under H_2O saturated conditions, displaying isopleths of the total H_2O content (mol%) of the mineral assemblages (i.e., not including the H_2O eventually present as a fluid phase in the pore spaces), in dashed white lines. The peak *P-T* conditions deduced for sample 20GP10 are shown by the red star at 1.9 GPa and 520 °C, as well as the hypothetic prograde path in dashed line. The blue star at 0.5 GPa and 600 °C indicates the Variscan amphibolite-facies *P-T* conditions for the Gran Paradiso Unit, after Le Bayon et al. (2006), for which a H_2O content of 5.7 mol% is calculated. Three grey arrows symbolizing geothermal gradients typical for subduction zone environments were added (6°, 10° and 15° per kilometer, calculated according to the standard ('lithostatic') assumption $P = \rho \cdot g \cdot z$, with ρ = 2.95 g·cm^{-3} and g = 9.81m·s^{-2}). Prograde increase in *P-T* conditions along either the three geothermal gradients or the hypothetic prograde path would lead to dehydration of the rock, whereas a protolith with a H_2O content corresponding to a Variscan amphibolite facies grade (5.7 mol% H_2O) would require hydration prior to peak *P-T* conditions. The dashed black line (labeled FSP out) shows the plagioclase-out reaction that should be crossed in order to reach thermodynamic equilibrium at high-pressure conditions.

Journal Pre-proof

Journal Pre-proof

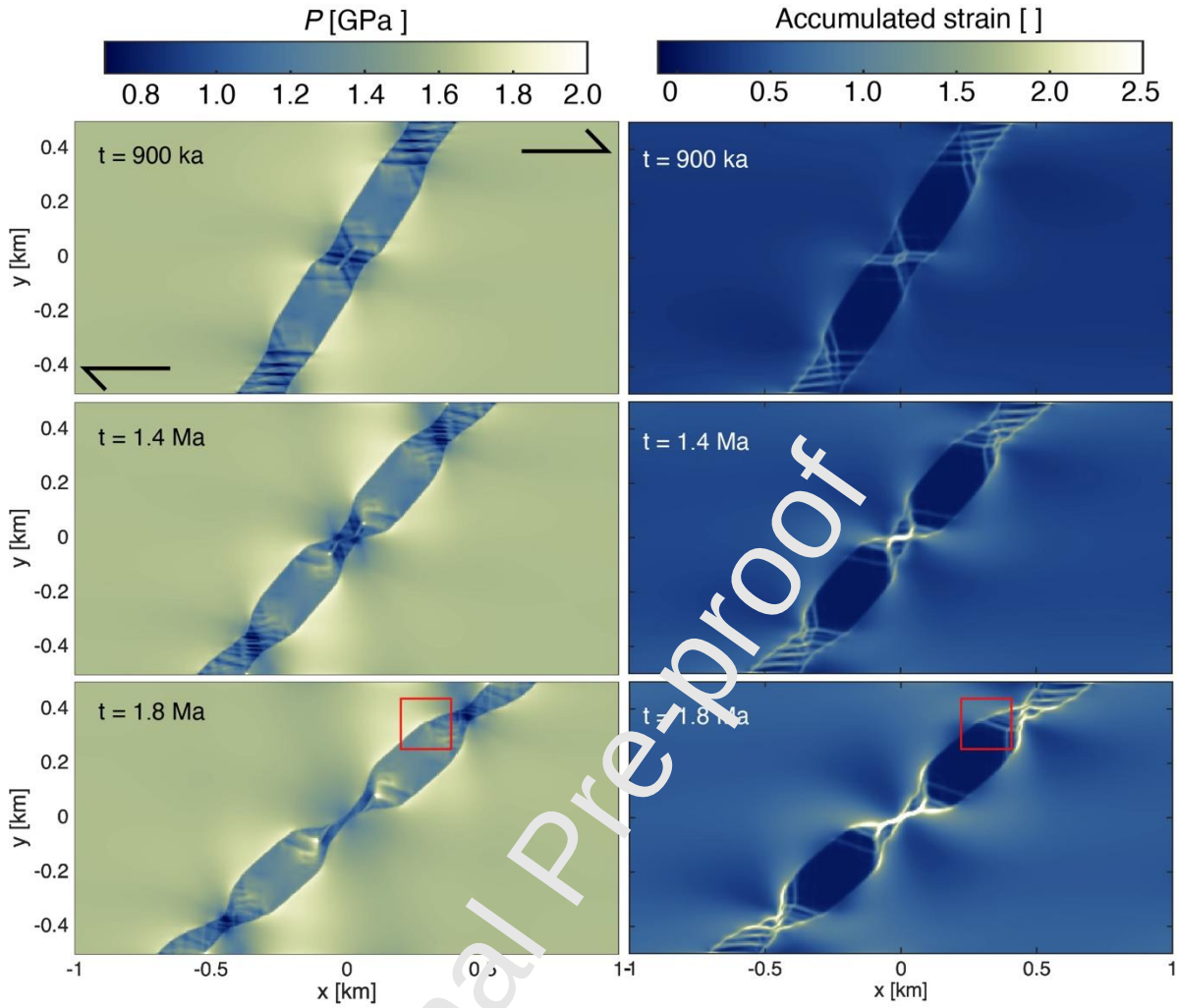

Figure 8 Pressure field [GPa] and accumulated strain at successive time steps of the simple shear deformation of a dry and strong layer within a wet and soft matrix. During shearing, necking localizes at the level of the soft inclusion, and progresses until a pinch-and-swell structure is formed. *P* field shows local deviations from the background *P*, with a lower *P* in the boudinaged layer than in the matrix. The accumulated strain is the lowest within the boudin cores and the largest in the necking zones. A square illustrates an area of the model that could be representative of the studied field area, where *P* is 0.4 to 0.6 GPa higher in the matrix than in the boudin, and the accumulated strain is high in the matrix and low in the boudin.

Journal Pre-proof

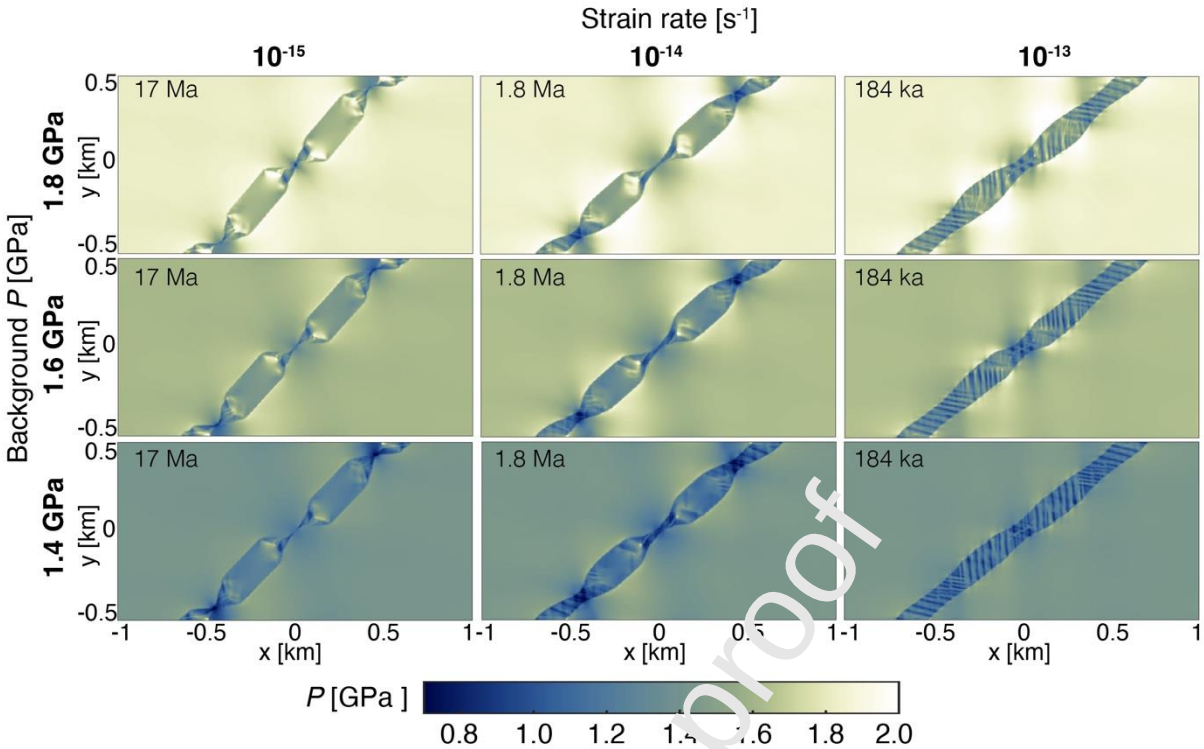

Figure 9 Effect of strain rate (10^{-15} to 10^{-13} s^{-1}) and background P (1.4 to 1.8 GPa) on the development of the pinch-and-swell structure and P field. For lower strain rates, deformation localizes mostly in the necking zones and boudins cores remain essentially undeformed, whereas for larger strain rates, shear bands develop inside the strong layer prior to necking. A variation of the background P does not significantly affect the shape of the structures but shifts the overall P field.

Journal Pre-proof

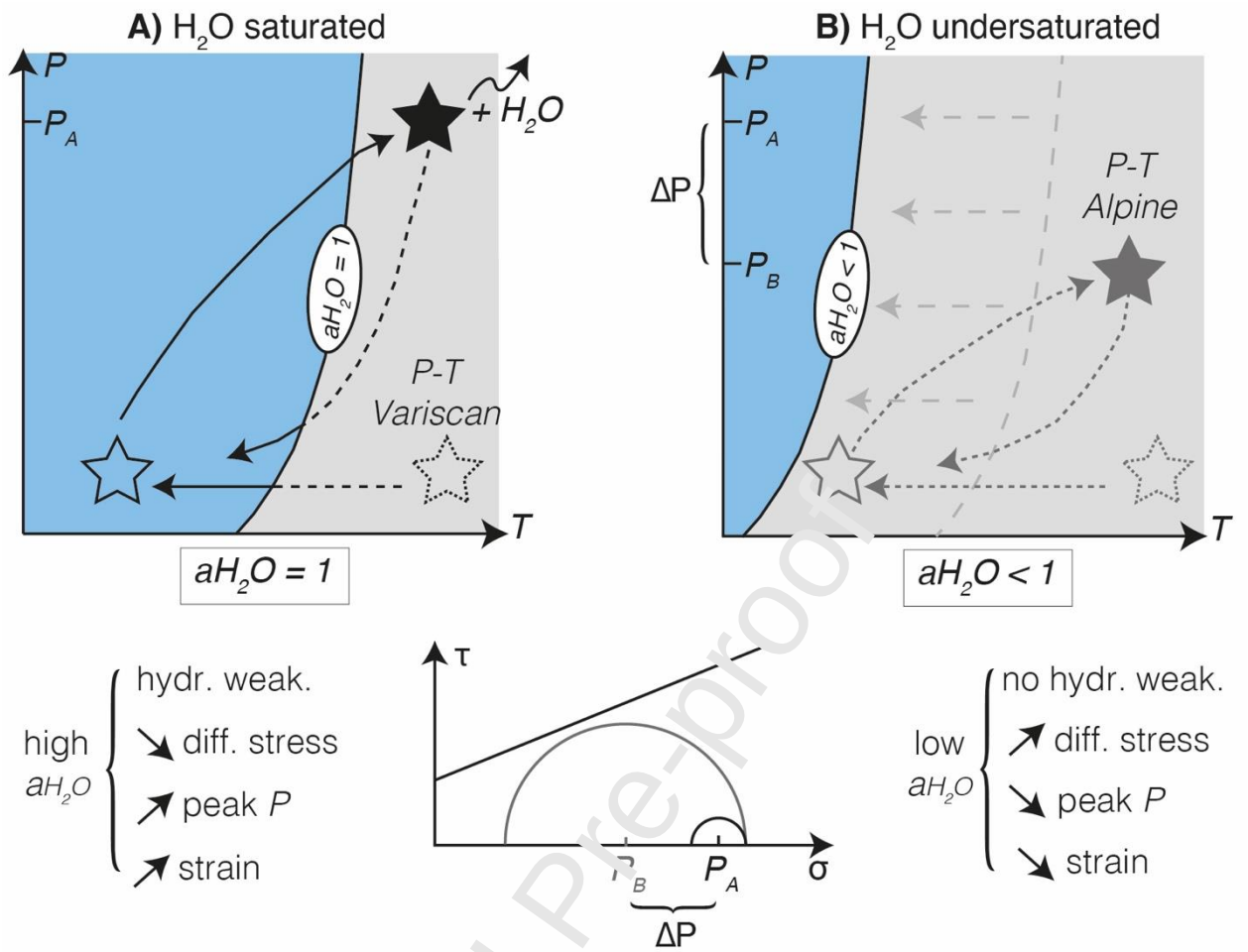

Figure 10 Simplified sketch illustrating the combined petrological and mechanical effects of contrasting H_2O (under)saturation conditions during the metamorphic evolution of two rocks in contact during Alpine orogeny. Case A) shows a H_2O saturated rock characterized by a unit H_2O activity ($aH_2O = 1$), such as the shear zone paragneiss, and case B) illustrates a H_2O undersaturated rock ($aH_2O < 1$), such as the low strain paragneiss. In both cases, the same dehydration reaction separates a hydrous field on the left (blue field), from an anhydrous field on the right side (gray field). The *P-T* trajectories are shown, starting from the Variscan stage (dashed star) at H*T*-L*P* conditions. Both rocks first cool down at the end of the Variscan orogeny, where they equilibrate to the pre-Alpine L*T*-L*P* condition (empty solid star). Mohr circle illustrate the differential stress in both rocks. Due to the contrasting stress state between rock A and B, at H*P* conditions, P_A, the *P* of rock A, corresponding to its mean stress, is higher than P_B, the *P* of rock B, leading to a *P* difference of $\Delta P = P_A - P_B$. Strain localizes in the weak rock and the strong rock remains mostly undeformed.

Journal Pre-proof

Competing interest declaration

The authors declare no competing interests.

Journal Pre-proof

Journal Pre-proof

Highlights

- H_2O saturation conditions impact not only the metamorphic evolution, but also the stress state and deformation

- Heterogeneous stress conditions develop during deformation of similar rocks with contrasting H_2O saturation conditions

- Metamorphic pressure variations can be recorded due to local variability in H_2O (under)saturation conditions

- The tectono-metamorphic history of polymetamorphic units constitutes a geological heritage that controls the future development of metamorphic assemblages and deformation

Journal Pre-proof